Chapter 4
Synthesis and Electrocatalysis of Pt-Pd Bimetallic Nanocrystals for Fuel Cells

Ruizhong Zhang and Wei Chen

4.1 Introduction

Over the past few decades, research on novel environment-friendly energy conversion devices and their potential applications has attracted extensive interest due to the depletion of fossil fuel reserves and thus the growing demand for efficient but low-cost renewable energy [1, 2]. Fuel cells, such as proton-exchange membrane fuel cells (PEMFCs), direct methanol fuel cells (DMFCs), and direct formic acid fuel cells (DFAFCs), have been considered as the most promising power sources because of high power density, high energy-conversion efficiency, and zero or low emission of pollutants [3–6]. For fuel cells, platinum (Pt) has received unremitting interest as an electrocatalyst because of the highest catalytic activity among the studied catalysts for electro-oxidation of small organic fuels on the anode and oxygen reduction on the cathode [7–10]. However, several issues arise from using pure Pt as fuel cell catalysts. First, Pt surfaces are easily self-poisoned by the strong adsorption of CO intermediates originated from small organic fuel oxidation, leading to a severe decrease in the catalytic performance [11, 12]. Second, using Pt as cathodic catalysts in DMFCs, methanol molecules crossover from anode to cathode may lower the ORR performance because of the mixed potentials formed from the simultaneous methanol oxidation and oxygen reduction [13–15]. Third, the limited reserve in nature and the resulting sky-rocketing price of Pt has become

R. Zhang
State Key Laboratory of Electroanalytical Chemistry, Changchun Institute of Applied Chemistry, Chinese Academy of Sciences, Changchun, Jilin 130022, China

University of Chinese Academy of Sciences, Beijing 100039, China

W. Chen (✉)
State Key Laboratory of Electroanalytical Chemistry, Changchun Institute of Applied Chemistry, Chinese Academy of Sciences, Changchun, Jilin 130022, China
e-mail: weichen@ciac.ac.cn

K.I. Ozoemena, S. Chen (eds.), *Nanomaterials for Fuel Cell Catalysis*,
Nanostructure Science and Technology, DOI 10.1007/978-3-319-29930-3_4

one of the major barriers for the wide commercialization of fuel cells [16]. To improve the catalytic activities and lower the costs of catalysts in fuel cells, much effort has been devoted to combining Pt with another metal that is less constrained in terms of reserve and economic dependence, to form bimetallic nanocatalysts. As compared to monometallic Pt, bimetallic Pt-based nanocrystals are expected to display not only a combination of the properties associated with two distinct metals, but also new and unexplored properties because of a possible bi-functional mechanism or the so-called ligand effect [17–19].

Among the metals around Pt in the periodic table, palladium (Pd) is probably the best candidate to generate bimetallic electrocatalysts with Pt due to the following obvious advantages. First, Pd and Pt share the same face-centered cubic (fcc) structure and almost identical lattice constants (with a mismatch of only 0.77%), both of which are beneficial to the formation of Pt-Pd bimetallic nanocrystals with single crystallinity. Second, the combination of Pt with Pd has a crucial impact on the electronic structure of Pt, resulting in superior electrocatalytic activities for a specific reaction owing to the formation of Pt-Pd bonds [20, 21]. According to the studies by Nørskov and co-workers [22–25], the strain and electronic coupling presented in a catalyst play a key role in determining the catalytic properties because both of the two parameters can result in shifts of the d-band center (calculated with respect to the Fermi level), which is directly related to the adsorption energies of reactants on a catalyst as well as their activation barriers. Of them, a compressive strain tends to down-shift the energy of the d-band center, causing adsorbates to bind less strongly to the catalyst, while a tensile strain has the opposite effect. On the other hand, the electronic coupling can result in shifts for the d-band center due to a change in the density of states near the Fermi level. As for Pt-Pd bimetallic catalysts, a small compressive strain resulting from their weak lattice contract can cause a downshift of the d-band center, thus lowering the binding strength for the adsorbed intermediates. As a consequence, the changes in the d-band properties of Pt caused by its combination with Pd, and the small mismatch in the lattice constants between Pt and Pd, makes Pt-Pd bimetallic nanocrystals attractive catalysts for various reactions. Taking ORR as an example, the rate-limiting step at high potential is the desorption of intermediates (O, OH, etc.) produced during the reaction. The weakened binding strength of the intermediates on a Pt-Pd bimetallic catalyst can activate the Pt sites required for the adsorption of O_2 and then the splitting of the O-O bond, therefore accelerating the kinetics of oxygen reduction [26]. In addition, a strong interaction between Pt and Pd due to the formation of Pt-Pd bonds can also change the electronic structure of Pt, causing the enhanced amount of O_2 adsorbed on the surface of Pt and thus improving ORR catalytic activity.

Moreover, it has been identified that the dissolution of Pt is a major reason for the degradation of catalysts in proton-exchange membrane (PEM) fuel cells due to the presence of dissolved molecular oxygen, highly aggressive condition in terms of acidic pH, and the highly positive potential for device operation [27]. Therefore, compared to other metals such as Ag, Cu, Co or Ni, the use of Pd may also help minimize the corrosion and loss of catalysts in an acidic environment such as the

medium of a PEM fuel cell [28]. Especially, the introduction of Pd can prevent the electrocatalysts from degradation to a certain extent by up-shifting the dissolution potential of Pt and thus assure long-term stability [29]. From these perspectives, it has been actively explored Pt-Pd bimetallic catalysts for a variety of reactions with enhanced performance.

In addition to elemental compositions, the size, shape and structure of Pt-Pd bimetallic system can also be finely manipulated to further enhance their catalytic performance. Since electrocatalytic reactions are very sensitive to the exposed crystal facets and the proportion of atoms located at the facets, edges or corners of catalysts, recent years tremendous efforts have been devoted to the syntheses of Pt-Pd bimetallic nanocrystals with well-defined shapes in high yields and purity by tuning various experimental parameters [30]. By using Pd nanocrystals as the seeds for overgrowth or sacrificial templates for galvanic replacement, Pt-Pd alloys with different structures/shapes including alloys, core-shell, dendrities, alternating multi-shells, and atomic monolayer, can be easily synthesized by different strategies. These preparation methods include co-chemical reduction and its combination with galvanic replacement to generate alloy nanocrystals, galvanic replacement between Pd nanocrystals and a Pt salt precursor for generating dendritic nanostructures, seed-mediated overgrowth for generating core-shell, multi-shell, and dendritic nanostructures, and a combination of electrochemical deposition and galvanic replacement for generating Pt monolayer on Pd nanocrystals, etc.

Besides the catalytic activity and costs, the stability and lifetime of an electrocatalyst are also critical issues for its practical applications in fuel cells. When Pt-Pd bimetallic nanocrystals are used as fuel cell catalysts, the catalyst support also plays an important role in determining the catalytic properties. For a catalyst support, it should have a high surface area for catalyst dispersion, a strong affinity to immobilize the catalyst particles, a high electrical conductivity to accelerate electron transfer in redox reactions, and a high electrochemical stability in acidic or alkaline electrolytes to ensure a stable structure. Up to now, various carbon materials including traditional carbon materials (e.g., Vulcan XC-72R carbon black) and nanocarbon materials (e.g., carbon nanotubes, graphene and ordered mesoporous carbon) have been used for the dispersion of catalyst particles. However, earlier studies have shown that except for the dissolution and aggregation of metal nanoparticles, the severe corrosion and oxidation of carbon support materials in the harsh operating environment could also lead to quick degradation of the electrocatalytic performance [31, 32]. Therefore, in recent years great efforts have also been devoted to addressing the challenges of catalyst supports via developing non-carbon support materials such as metal oxides, electronically conductive polymer, nitrides and carbides [33].

Herein, we will first summarize recent progress in the development of experimental techniques for the preparation of unsupported/supported Pt-Pd bimetallic nanocrystals with unique structures, and then focus on their applications in fuel cells as anode and cathode catalysts.

4.2 Synthesis of Pt-Pd Bimetallic Nanocrystals

It is well-known that the catalytic activities of nanoparticle electrocatalysts are strongly dependent on their composition, shapes, size, exposed surface planes and the interactions between nanocrystals and catalyst supports. In the past few decades, various methods have been applied in the synthesis of Pt-Pd bimetallic nanocrystals with structures in the form of alloy, core-shell, dendrities, multi-shells, and supported monolayer. These well-defined Pt-Pd nanostructures can be generally prepared through co-chemical reduction, galvanic replacement, seed-mediated growth and electrochemical deposition synthetic routes. Typically, co-chemical reduction synthesis of Pt-Pd bimetallic nanocrystals refers to the reduction of Pt and Pd precursors in the presence of capping agents and/or stabilizers. Pt-Pd nanoalloys can also be obtained through *in situ* oxidation and dissociation of Pd nanocrystals by galvanic replacement with a Pt salt precursor. For a seed-mediated growth approach, the well-defined shapes of Pt or Pd as seeds for epitaxial growth of a Pd or Pt-shell. It is also feasible to control the shell by using electrochemical deposition methods. In this section, we summarize various leading synthetic techniques and the formation mechanisms for the preparation of Pt-Pd nanocrystals.

4.2.1 Co-chemical Reduction Method

In the past decades, co-chemical reduction has proved to be a straightforward strategy for the facile synthesis of bimetallic nanocrystals. With this technique, it is feasible to achieve simultaneous reduction of both Pt and Pd salt precursors in the presence of a capping agent and/or a stabilizer due to their similar electrochemical potentials of 0.74 V (versus a reversible hydrogen electrode) for $PtCl_6^{2-}$/Pt and 0.62 V for $PdCl_4^{2-}$/Pd. The obtained Pt-Pd bimetallic nanocrystals are interesting for various electrocatalytic reactions due to the co-existence of Pt and Pd atoms on the nanocrystal surfaces [34]. To date, various reducing agents have been used to co-reduce Pd and Pt salt precursors for the synthesis of Pt-Pd alloy nanocrystals, including sodium borohydride, alcohol, formic acid, formaldehyde, hydrazine, ascorbic acid, etc. By using sodium borohydride ($NaBH_4$) as a reductant, Crooks and coworkers [35] prepared Pt-Pd bimetallic nanoparticles via the co-reduction of K_2PtCl_4 and K_2PdCl_4 in a poly(amidoamine) dendrimer (G6-OH) aqueous solution. Two steps are involved in the process: (i) loading Pt and Pd ions into the dentrimers by fully complexing with the interior amines of dendrimers, and (ii) co-reducing the complexed Pd and Pt ions by $NaBH_4$. Interestingly, the synthesized bimetallic Pt-Pd nanoparticles by this process have almost the same diameter (~1.8 nm) containing an average of 180 atoms but with seven different Pt/Pd ratios. Here, the dendrimer template plays a vital role in controlling the size of Pt-Pd nanoparticles (smaller than 3 nm) and the composition variation (molar ratios adjustable from 1:5 to 5:1). TEM and single-particle energy-dispersive

spectroscopy (EDS) indicated that the calculated particle diameter and Pt/Pd ratios in the Pt and Pd precursors are very consistent with the measured ones. Therefore this dendrimer-templating is a unique method for preparing nanoparticles having particular Pt/Pd ratios, uniform size and composition. In another work, one-dimensional ultrathin Pt-Pd alloy nanowires were synthesized in a cetyltrimethylammonium (CTAB)-assisted water-chloroform micelles system [36]. In this synthesis, a mixed aqueous solution of Pt and Pd salts was mixed with a chloroform solution of CTAB, followed by the addition of a $NaBH_4$ aqueous solution. In the mixed solution, the reduction of precursor ions and metal growth occurred in the swollen wormlike micelle networks of chloroform droplets with the CTAB molecules. Because of the strict limitation of the wormlike micelle networks, the obtained Pt-Pd nanowires showed an average size of 2.5 nm with a narrow diameter distribution, and both Pt and Pd can be co-reduced to form alloy with an atomic ratio of about 1:1, as confirmed by EDX measurements.

When Pt-Pd bimetallic materials are used as fuel cell catalysts, they are usually dispersed on a catalyst support. Among the used catalyst supports, Vulcan XC-72 carbon black is the most popular carbon support for immobilizing and stabilizing Pt-Pd nanoparticles [37–44], while carbon nanotubes [45–48], conducting polymer composite matrix [49], and tungsten carbide [50] have also been explored as potential supporting materials. For instance, Zhang et al. [51] synthesized a series of Pd_xPt_{1-x} nanoparticles dispersed on carbon black by reducing the mixture of Pd (II) and Pt(II) precursors by $NaBH_4$ in the presence of Vulcan XC-72 carbon. In the synthesis, EDTA was also used as a chelator for Pd and Pt ions to ensure the co-reduction of Pd(II) and Pt(II) species. The highly dispersed Pd_xPt_{1-x} nanoparticles on carbon black exhibited composition-dependent catalytic activity for formic acid electro-oxidation and the $Pd_{0.9}Pt_{0.1}$ nanoparticles with a mean size of 3.2 nm showed the best performance among the series.

In addition to strong reducing agents, Pt-Pd bimetallic nanostructures have also been prepared by a polyol process, in which mild reductants such as ethylene glycol [52–68], methanol [69], glycerol [70, 71], and 1,4-butanediol [53], have been used. It is well-known that Pt nanocrystals with different exposed surfaces have different electronic structures and surface atomic arrangements, and the appropriate crystal phase and/or composition can greatly enhance reaction kinetics due to the minimized surface energy and total excess free energy. Therefore, much work has been done to prepare shape-controlled metallic nanostructures with desired exposed crystal facets. For instance, Lee and co-workers [72] reported a glycerol reduction method to synthesize Pt-Pd nanoparticles exhibiting dominantly exposed (1 1 1) facets in octahedral shape with complete alloy formation between Pt and Pd metallic phases. During the fast reduction process, the thermodynamically minimized crystalline surface energy and thus the formation of crystal facets with a low surface energy in the Pt-Pd structure can improve the electrocatalytic performance of the obtained carbon supported Pt-Pd nanoparticles composite toward methanol oxidation. By using a hollow-core mesoporous shell (HCMS) carbon as support, Berker et al. [65] reported a rapid method to synthesize Pt-Pd/HCMS composite by the co-reduction of H_2PtCl_6 and $PdCl_2$ using ethylene glycol as a reducing agent

under microwave irradiation. It was proposed that the HCMS carbon facilitated the diffusion of hydrogen and oxygen as well as the water transport within fuel cells, leading to significantly improved fuel cell performance. Formic acid has also been used to synthesize Pt-Pd bimetallic nanocrystals [73–75]. Guo et al. [76] demonstrated a simple procedure to synthesize Pt/Pd hybrid supported on polyaniline (PANI) nanofibers with high conductivity and surface-to-volume ratios. In this method, the PANI nanofibers were first synthesized by a wet-chemical approach and then the as-obtained 1D PANI nanofibers were added into a mixture containing H_2PtCl_6 and H_2PdCl_4. HCOOH was finally injected into the above mixture to reduce the precursors at room temperature. The SEM and TEM images shown in Fig. 4.1a, b indicate that a large number of PANI nanofibers with a diameter of 60–100 nm have been obtained. Compared with the smooth surface of pristine PANI, a rougher surface of the as-prepared PANI/Pt and PANI/PtPd indicates that Pt (Fig. 4.1c, d) and PtPd nanoparticles (Fig. 4.1e, f) have been successfully deposited on the surface of PANI fibers. Moreover, the corresponding magnified images further revealed that the small PtPd nanoparticles formed a network and thus leading to many nanoporous structures on the surface of hybrid nanofibers, which favor a high electrocatalytic activity.

Most recently, by using graphene as support, Wang and co-workers [77] used the formic acid method to prepare graphene-supported 1D PtPd nanorods (G-PtPd NRs) by co-reducing H_2PtCl_6 and $Pd(NO_3)_2$ in the presence of HCOOH. In comparison with the carbon-supported PtPd NRs and graphene-supported Pt NRs, the G-PtPd NRs showed a larger diameter of about 4.4 nm and a longer length of about 35 nm measured from the corresponding TEM images. Extended X-ray absorption fine structure (EXAFS) studies confirmed the formation of G-PtPd alloy with a Pt-rich inner core and a Pd-rich outer shell. XRD patterns indicated that the growth of (111) and (220) planes of G-PtPd NRs was promoted for the alloying of Pt and Pd on graphene support. In addition, the results of X-ray absorption near edge spectroscopy (XANES) also showed that using graphene as a support and alloying with Pd synergistically modified the d-band of Pt, and the total number of unoccupied d-states for G-PtPd was reduced to as low as 0.295. All these results suggested that the G-PtPd had lower unfilled d-states and more d-band electrons were transferred from Pd to Pt, resulting in enhanced ORR performance.

Meanwhile, a simple microemulsion method was also developed to construct Pt-Pd nanoparticles [78, 79]. With this technique, the preparation of metal nanoparticles is realized by mixing two different micro-emulsions carrying the specific reactants (metallic salts and reducing agent) dissolved in aqueous phase. Microemulsion method has been accepted to be a unique method for the production of metal particles with a very narrow size distribution. For example, Escudero and coworkers [80] prepared alloyed Pt-Pd nanoparticles by reducing H_2PtCl_6 and $PdCl_2$ with hydrazine in a water-in-oil micro-emulsion of water/Berol 050/*iso*-octane. The obtained Pt-Pd nanoparticles were smaller than 5 nm and exhibited potential application in fuel cells.

In recent years, microwave-assisted technique has also been applied to the synthesis of metal nanoparticles [81]. Compared with the traditional chemical

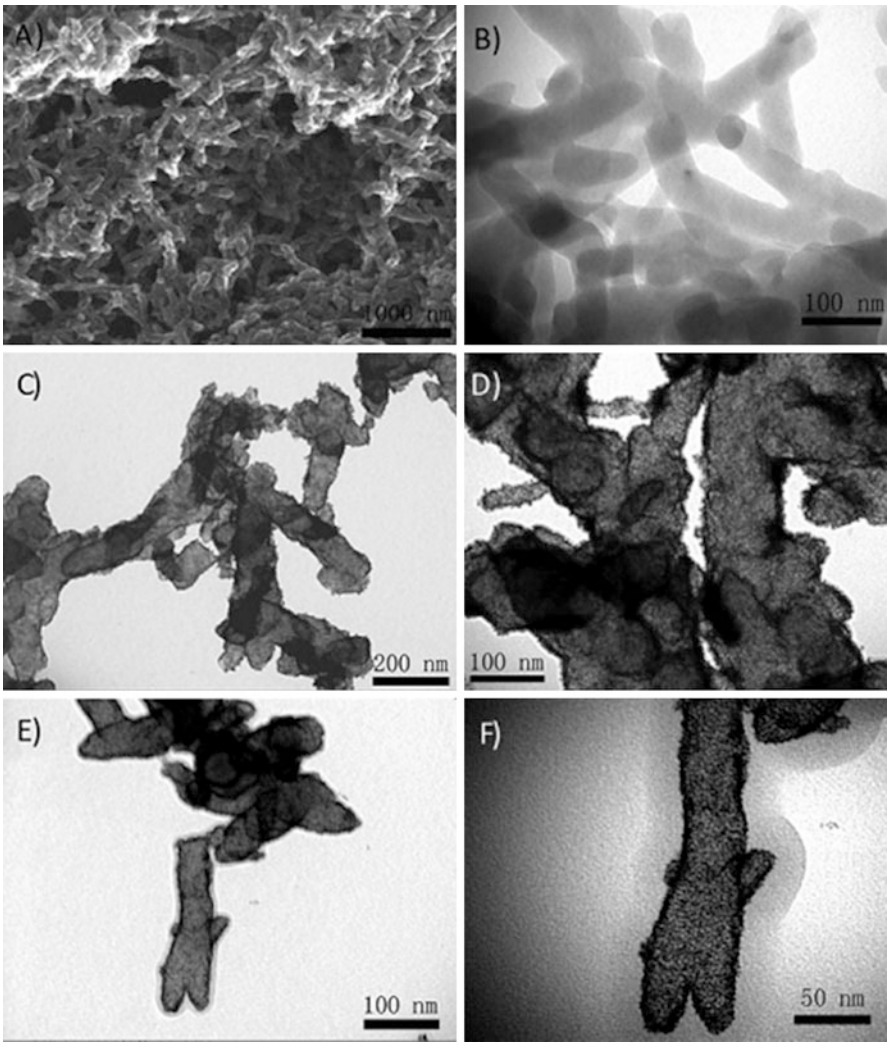

Fig. 4.1 (**a**) SEM and (**b**) TEM images of PANI nanofibers. (**c**, **d**) TEM images of PANI nanofiber-supported supra-high density Pt NPs. (**e**, **f**) TEM images of PANI nanofiber-supported Pt/Pd NPs at different magnifications. Reprinted with permission from [76]. Copyright 2009 Wiley-VCH

methods, the microwave heating provides homogeneous reaction conditions and a fast kinetic process. Zhang and coworkers [82] reported a simple method to synthesize three-dimensional Pd@Pt core-shell nanostructures with a high yield via the co-reduction of K_2PtCl_4 and $PdCl_2$ in the presence of CTAB by using ascorbic acid as a reducing agent under microwave irradiation. It was shown that the long alkyls of CTAB served as a shape-control agent to tailor the structure and improve the dispersion of nanoparticles in the synthesis. TEM and SEM

characterizations showed that the morphology of the synthesized Pd@Pt nanostructures can be easily controlled by changing the molar ratio between Pt and Pd precursors. And the Pd@Pt morphology was changed from cubic to spherical shapes by decreasing the Pd/Pt molar ratio (3:1 to 1:3). The authors also studied the shape effect on the eletrocatalytic activity for MOR and ORR, and among the different Pd@Pt nanostructures, the sample at a Pd/Pt molar ratio of 1:3 exhibited the best catalytic activity.

Interfacial self-assembly was found to be a simple and effective strategy for the synthesis of noble metal nanomaterials, and the liquid-liquid, liquid-air and oil-water-air interfaces have showed promise as flexible 2D platforms for nanoparticles assembly [83–87]. Wu et al. [88] prepared macroscopic free-standing Pd/Pt nanomembranes (Pd/Pt-FNMs) with well-defined monolayer structures as large as several square centimeters by one-step self-assembly at a water-air interface. In the synthesis, aqueous solutions of $PdCl_2$, K_2PtCl_6 and sodium citrate (Na_3CA) were mixed in a beaker. Subsequently, the reducing agent $NH_2OH{\cdot}HCl$ was quickly added into the above solution. After boiling for 15 min and then cooling down to room temperature, a monolayer of macroscopic Pd/Pt-FNMs floated at the water-air interface and covered the solution surface of the whole beaker. The composition of the Pd/Pt-FNMs ($Pd_{53}Pt_{47}$-FNMs, $Pd_{33}Pt_{67}$-FNMs, and $Pd_{15}Pt_{85}$-FNMs) was easily tuned by adding a different amount of precursors and confirmed by ICP-AES. From the TEM images, the obtained Pd/Pt-FNMs exhibited similar well-defined morphologies, and Fig. 4.2a–c shows the details of the $Pd_{33}Pt_{67}$-FNMs. It can be seen that the Pd/Pt nanoparticles have a uniform size with an average diameter of 9.25 nm. Although no obvious grain boundaries between Pd and Pt are observed from the high-resolution TEM (HRTEM) measurements (Fig. 4.2d), the bimetallic nature of the FNMs can be clearly seen from the high-angle annular dark-field (HDDAF-STEM) image and the nanometer-scale TEM elemental mapping images (Fig. 4.2e). In the mechanistic study, the authors found that when increasing the dosage of Na_3CA, Pd/Pt nanomembranes failed to form at the water-air interface. However, with decreasing dosage of Na_3CA, highly aggregated nanostructures were produced. Therefore, the presence of an appropriate dosage of Na_3CA was believed to be the key to achieve high-quality Pd/Pt-FNMs.

In another study, Sun and coworkers [89] reported an oil-phase method for the synthesis of polyhedral Pd-Pt alloy nanocrystals with a controlled size (3.5–6.5 nm) and composition ($Pd_{88}Pt_{12}$ to $Pd_{34}Pt_{66}$). This synthesis involves co-reduction of Pd $(acac)_2$ and $Pt(acac)_2$ with morpholine borane (MB) in oleylamine (OAm) at different temperatures. The TEM and HAADF-STEM images confirmed the formation of single-crystal nanoparticles in high yield with a uniform size. Both Pd and Pt are uniformly distributed throughout each particle from EDX mapping measurements. The linear dependence with a nearly unity slope implies that the two precursors were co-reduced at the same rate in generating the bimetallic nanocrystals. The formation of a single complex between the Pt and Pd precursors with the capping agent facilitates the simultaneous reduction in an elevated oil-phase. In a typical synthesis, the composition of the Pt-Pd alloy nanocrystals could be adjusted by controlling the amounts of $Pd(acac)_2$ and $Pt(acac)_2$ added into

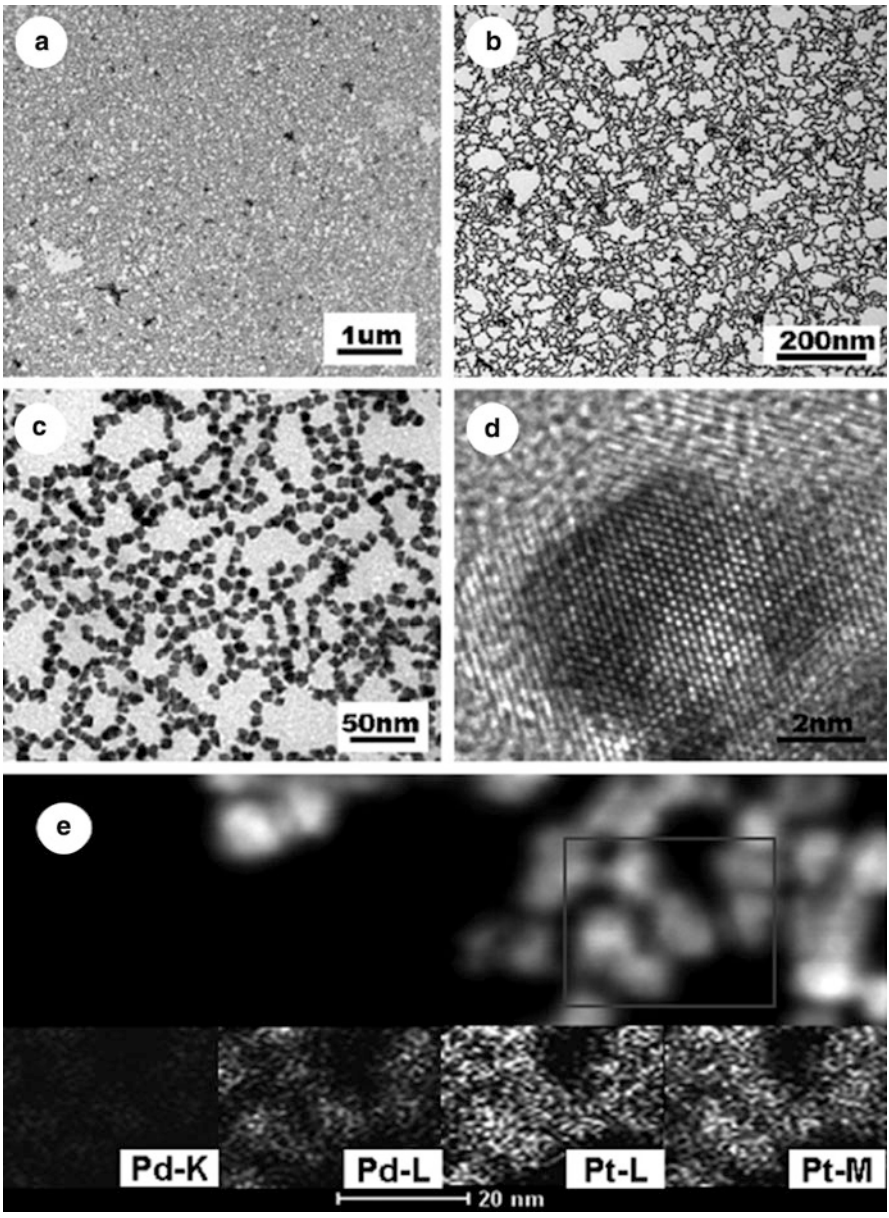

Fig. 4.2 (**a**–**c**) TEM images, (**d**) HRTEM image, and (**e**) HAADF-STEM image and the corresponding nanometer-scale TEM elemental mapping (*inset*) of the $Pd_{33}Pt_{67}$-FNMs. Reprinted with permission from [88]. Copyright 2012 Wiley-VCH

the reaction solution. More importantly, at a constant composition, the size of the Pt-Pd nanocrystals could be easily tuned by varying the temperature at which MB was injected. When MB was injected at 40, 60 and 80 °C, 6.5, 5 and 4.5 nm $Pd_{67}Pt_{33}$ nanoparticles can be formed, respectively. The as-synthesized Pt/Pd nanoparticles exhibited highly composition-dependent catalytic activities and high stability for methanol oxidation reaction in acid media.

Although great success has been achieved in the synthesis of Pt-Pd alloy nanoparticles via the afore-mentioned techniques, the products from these syntheses were largely restricted to small nanoparticles (typically less than 5 nm in size) with poorly defined crystallinity and morphology. By heating an aqueous solution containing Na_2PdCl_4, K_2PtCl_4 and poly (vinyl pyrrolidone) (PVP) at 80 °C for 18 h, Xia and coworkers [90] demonstrated a co-reduction approach for the synthesis of Pt-Pd alloy nanocrystals with well-defined shapes and twinned structures. In this process, the commercially available PVP was employed as a weak reducing agent to manipulate the reduction kinetics owing to its hydroxy (OH)-end groups. It was found that the slow reduction rate associated with the weak reducing power of PVP is the prerequisite for the formation of Pt-Pd alloy nanocrystals with twinned structures. From the TEM characterizations in Fig. 4.3a, b, the formed Pt-Pd nanocrystals are mainly star-shaped decahedra with an average size of 40 nm and triangular nanoplates with lateral dimensions of 30–50 nm, as well as a small fraction of other shapes such as octahedra. The compositional line profiles of Pd and Pt on a star-shaped decahedron shown in Fig. 4.3c indicate the formation of Pt-Pd alloy. The HRTEM image (Fig. 4.3d) confirms the presence of fivefold twins from the center of a star-shaped decahedron. In this work, the PVP-mediated slow reduction rate could help retain the particles at small sizes for a long period of time before nucleation. During the period, the small particles easily coalesced into larger particles to reduce surface-to-volume ratio, leading to the formation of twinned structures. When the reaction was conducted using a relatively high-rate reducing agent of ethylene glycol, Pt-Pd nanocrystals with a truncated, octahedral shape were produced, and this fast reduction process favored the formation of Pt-Pd nanocrystals with a single-crystal structure.

Hydrothermal method is another useful and frequently used technique for the preparation of Pt-Pd nanocrystals with the advantages of simplicity, free of templates, and easy shape-control of metal nanocrystals [91–93]. For instance, Yan and coworkers [94] demonstrated a shape-selective synthesis of Pt-Pd nanotetrahedrons (NTs) and nanocubes (NCs) with less than 10 nm in size via a one-step hydrothermal process by using small ions as efficient facet-selective agents (Fig. 4.4a). With a combination of $Na_2C_2O_4$ and formaldehyde as the (1 1 1) facet-selective agent and reducing agent, single-crystalline Pt-Pd NTs enclosed by four (1 1 1) facets with a shape selectivity of ~70 % and an average size of 4.9 nm were produced (Fig. 4.4b). The selective adsorption of $C_2O_4^{2-}$ species on the (1 1 1) facets was found to be a critical factor in directing the formation of Pt-Pd NTs. In comparison, Pt-Pd NCs (~8.5 nm) with a shape selectivity of about 88 % were produced in the presence of both large amount of Br^- and tiny amount of I^- anions owing to their selective capping for the (1 0 0) facet (Fig. 4.4c). Furthermore, reduction rate dependent on

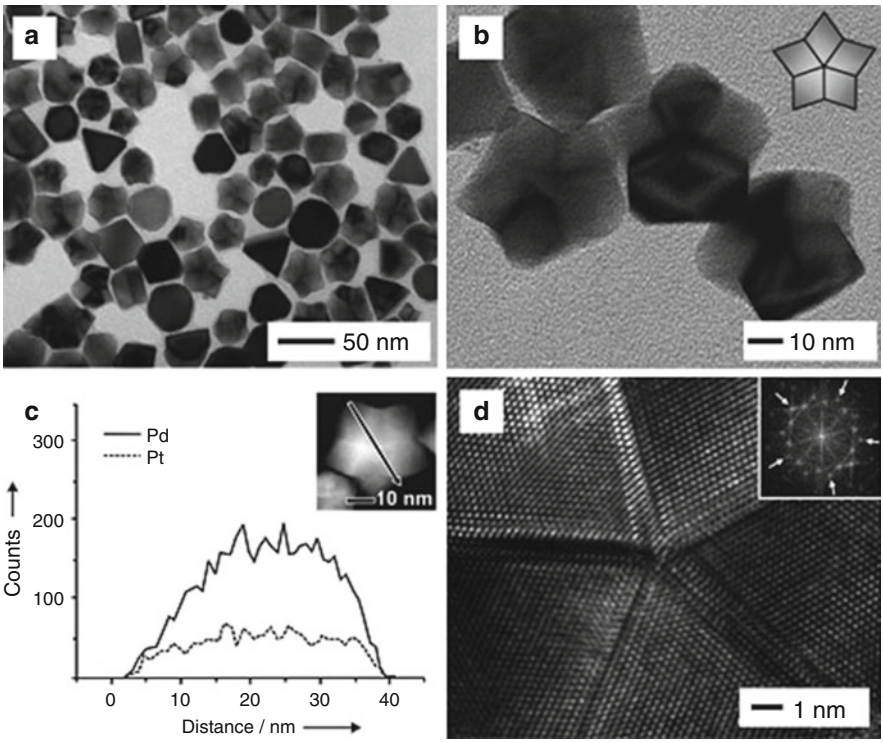

Fig. 4.3 (**a**, **b**) TEM images, (**c**) EDX line-scan, and (**d**) HRTEM image of Pt-Pd alloy nanocrystals synthesized by co-reduction of Na_2PdCl_4 and K_2PtCl_4 with PVP in an aqueous solution. The inset in (**b**), (**c**) and (**d**) correspond to schematic illustration, the HAADF-STEM image, and the Fourier transform pattern of the star-shaped decahedron, respectively. Reprinted with permission from [90]. Copyright 2009 Wiley-VCH

the type of reductant also played a vital role in determining the shape of the Pt-Pd products. A fast enough reducing rate by using a certain amount of formaldehyde could improve the shape- and size-uniformity of the obtained Pt-Pd NTs, while a slow reduction rate (with PVP instead of formaldehyde as the reducing agent) was found to be beneficial to the formation of regularly shaped Pt-Pd NCs. The electrocatalytic studies showed that the obtained alloy nanocrystals exhibit enhanced and facet-dependent catalytic activity and stability for methanol electrooxidation in the order of NCs > NTs > commercial Pt/C.

Besides the intrinsic catalytic properties of catalysts, the support used also plays important roles in determining their catalytic performance. Due to the high electronic conductivity and large surface area, graphene has been recently used as a support material for Pt-Pd nanocrystals dispersion. Our group developed a facile hydrothermal method for the one-pot fabrication of reduced graphene oxide (rGO)-supported Pt-Pd alloy nanocubes (PtPd/rGO) [95]. In a typical procedure, $Pd(acac)_2$ and $Pt(acac)_2$ were mixed with PVP, and NaI in DMF solution of graphene oxide.

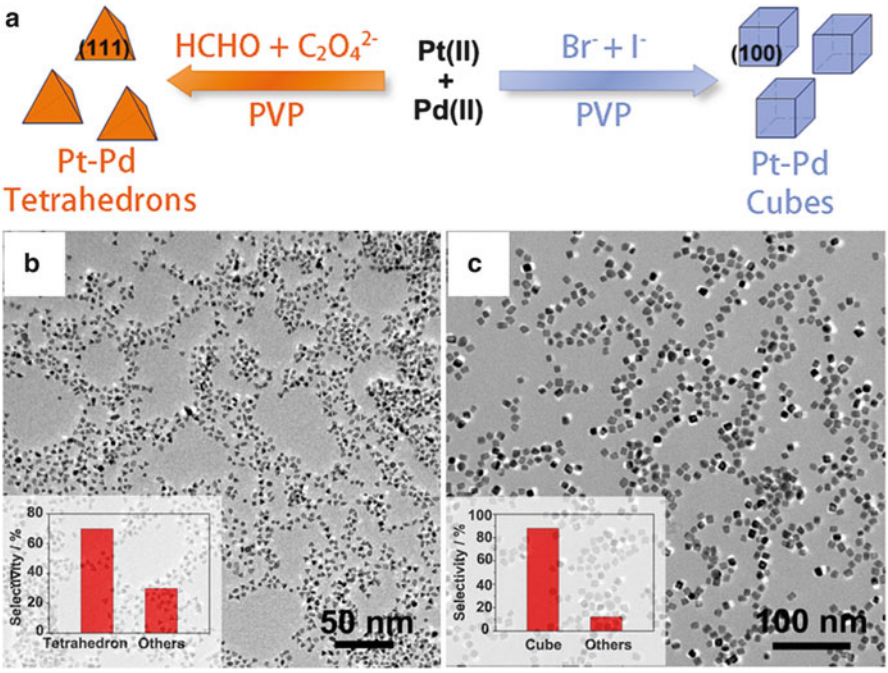

Fig. 4.4 (**a**) Schematic illustration of shape-controlled synthesis of Pt-Pd alloy nanocrystals with tetrahedral and cubic shapes. (**b**, **c**) TEM images of Pt-Pd tetrahedrons and cubes, respectively. The insets in (**b**) and (**c**) show the percentages of the alloy tetrahedrons and cubes, respectively. Reprinted with permission from [94]. Copyright 2011 American Chemical Society

After ultrasonic treatment, the mixed solution was then transferred to a Teflon-lined stainless steel autoclave and heated at 150 °C for 8 h. In this process, two key steps were included: (1) the reduction of graphene oxide (GO) and the nucleation of nanocrystals attached onto the surface of rGO, and (2) the gradual nuclei growth into cubic shapes under the protection of PVP. From HRTEM images and elemental mapping shown in Fig. 4.5a–g, single-crystalline Pt-Pd nanocubes with shape selectivity of 82% and an average size of 8.5 nm were uniformly distributed on the rGO surface. More recently, using GO as both a support material and a structure- and/or morphology-directing agent, rGO-supported PtPd concave nanocubes have also been successfully synthesized through a simple hydrothermal process [96]. In sharp contrast, only cubic PtPd alloy nanocrystals were obtained in the absence of GO. The as-prepared PtPd concave nanocubes exhibited enhanced electrocatalytic activity and durability toward methanol oxidation owing to the exposed high-index facets of {730} and the strong interaction between the catalysts and graphene support.

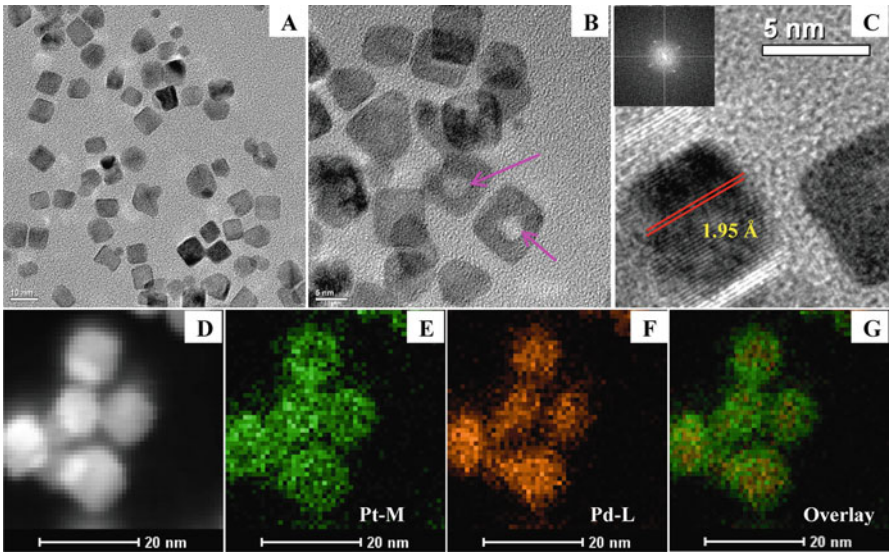

Fig. 4.5 (**a**–**c**) High-resolution TEM micrographs of the PtPd alloy nanocubes supported on rGO at different magnifications. The inset in (**c**) shows the FFT pattern of an individual PtPd nanocrystal. (**d**) The high-angle annular dark-field (HAADF)-STEM image of PtPd/rGO and the corresponding elemental mapping of (**e**) Pt, (**f**) Pd, and (**g**) the overlay. Reprinted with permission from [95]. Copyright 2013 American Chemical Society

4.2.2 Galvanic Replacement and Its Combination with Chemical Reduction

Galvanic replacement is a simple and popular route for controllably constructing various types of bimetallic nanocrystals. Compared with the co-chemical reduction method, galvanic replacement is based on an etching process without using hazardous reducing agents. Therefore, this technique is considered to be a green method for nanocrystals preparation. A galvanic replacement reaction is driven by the different electrochemical potentials between a sacrificial metal template and another metal ion in a solution phase. Typically, this process involves oxidation and dissolution of the template accompanied by reduction of another metal ions and deposition of the resultant atoms on the surface of template. Moreover, the size and morphology of the final product can be easily manipulated by using sacrificial templates with different size and shape and/or by controlling the extent of replacement reaction.

In recent years, galvanic replacement has been applied to the synthesis of supported- and unsupported-PtPd bimetallic nanocrystals [97–100]. By using Ag nanowires as sacrificial templates, Chen et al. [101] synthesized Pt-Pd nanotubes (PtPd NTs) with an average diameter of 45 nm, wall thickness of 7 nm and length of 10 μm. In this synthesis, Ag nanowires were first prepared via a polyol method, and the PtPd NTs were subsequently obtained by a galvanic replacement reaction

between Ag nanowires and the mixture of $Pt(CH_3COO)_2$ and $Pd(CH_3COO)_2$ in an aqueous solution. The as-prepared supportless-PtPd NTs exhibited enhanced catalytic activity and much improved durability for ORR compared to Pt NTs and the commercial Pt/C, which can be ascribed to their unique dimensions (i.e. micrometer-sized length) and anisotropic morphologies.

In theory, galvanic replacement reaction can occur between any pair of metals with appropriate difference in their redox potentials. In spite of the large difference in redox potential between $PtCl_6^{2-}$/Pt and $PdCl_4^{2-}$/Pd, it was found that no obvious galvanic replacement reaction occurs between Pd nanocrystals and $PtCl_6^{2-}$ ions unless under special reaction conditions. Xia and co-workers [102, 103] reported that the presence of Br^- ions could promote the initiation of galvanic replacement between $PtCl_6^{2-}$ ions and Pd nanocrystals. Interestingly, the Br^--induced galvanic replacement exhibited a preferential selectivity towards the (100) facets of Pd nanocrystals, resulting in the formation of Pt-Pd bimetallic nanocrystals with a concave structure due to the simultaneous dissolution of Pd atoms from the (100) facets and deposition of Pt atoms on the (111) facets. Figure 4.6 shows the typical TEM images of Pt-Pd nanocrystals synthesized via galvanic replacement reaction with different reaction times using Pd nanocubes as templates. As illustrated by the schematic drawings in the insets, the Pt-Pd nanocrystals evolved from Pd truncated cubes to Pt-Pd concave cubes and Pt-Pd octapods. The Pt-Pd nanocrystals can also be manipulated in terms of both morphology and size by using Pd templates with different sizes and shapes [102]. More interestingly, when a reducing agent of citric acid (CA) was introduced into the above system, Pt-Pd bimetallic nanocages rather than concave nanocrystals were generated [103]. In the process, it was suggested that two important stages were included: (1) Br^--induced selective galvanic replacement reaction between (100) facets of Pd nanocubes and $PtCl_4^{2-}$, resulting in the formation of Pt-Pd concave nanocubes; (2) co-reduction of Pd^{2+} ions evolved from the galvanic replacement, together with $PtCl_4^{2-}$ ions remained in the solution by CA into atoms and the subsequent deposition of these atoms on the side faces of the concave nanocubes. Thus, Pt-Pd alloy nanocages with cubic morphology could be easily obtained *via* a combination of Pd dissolution (related to galvanic replacement) and the following Pt-Pd overgrowth (due to co-reduction).

In a recent study [104], our group also investigated the galvanic replacement between Pd nanowires and $PtCl_6^{2-}$ in aqueous solution. PtPd alloy nanorods with a porous structure were successfully synthesized through this bromide-induced galvanic replacement route. The obtained PtPd nanorods showed much larger electrochemically accessible surface area compared with the Pd nanowires and commercial Pt/C, making them promising for application in fuel cells as cathode catalysts.

Despite great success achieved in the synthesis of Pt-Pd nanostructures *via* the afore-mentioned strategies, a key procedure for the synthesis of Pd templates is required. Zheng and co-workers [105] reported a one-pot fabrication of hollow Pt-Pd nanocubes by using a mixed precursors of $Pd(acac)_2$ and $Pt(acac)_2$, with a PVP and NaI solution in DMF. In this synthesis, because of the strong coordination of I^- ions to Pd^{2+} ions, the addition of I^- ions into the mixture of $Pd(acac)_2$ and

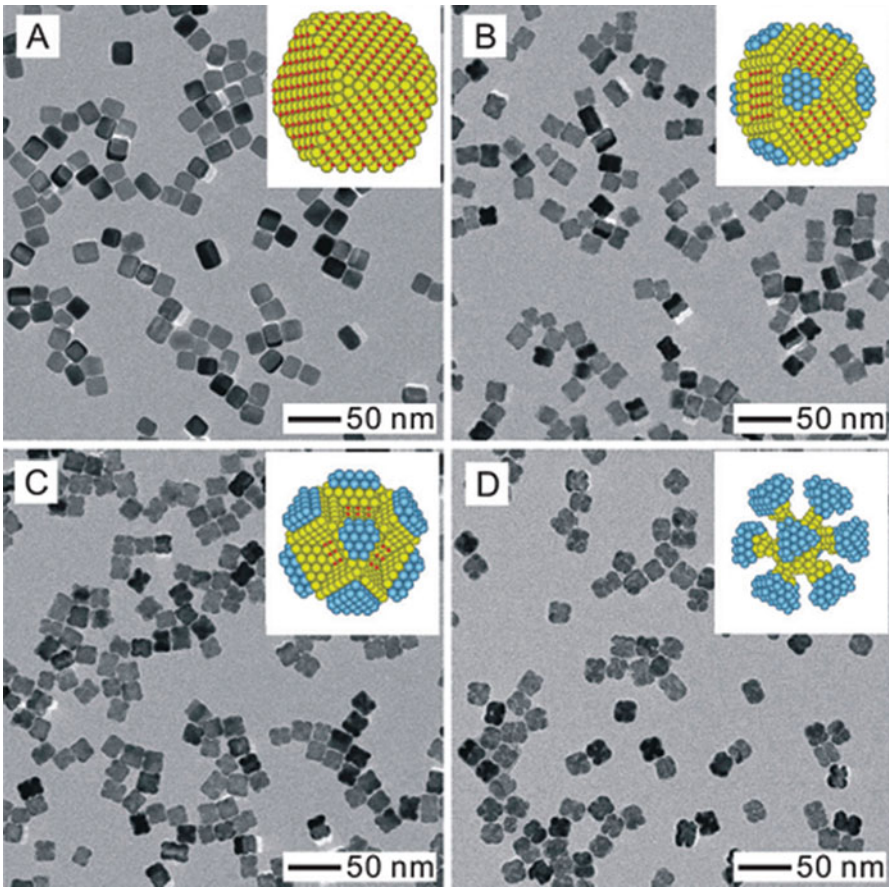

Fig. 4.6 TEM images of Pt-Pd nanocrystals in the form of nanocubes, concave nanocubes, and octapods that were formed through bromide-induced galvanic replacement at various reaction times: (**a**) 0.5, (**b**) 4, (**c**) 9, and (**d**) 20 h. The *yellow*, *blue* and *red* balls represent Pd atoms, Pt atoms, and Br^- ions, respectively. Reprinted with permission from [102]. Copyright 2011 American Chemical Society

$Pt(acac)_2$ can generate the new dominating precursors of PdI_4^- and $Pt(acac)_2$. In the DMF solution, PdI_4^- is more favorably reduced to form Pd nanocubes, and the galvanic replacement between temporal Pd nanocubes and Pt^{2+} species occurred subsequently to produce hollow Pt/Pd nanocubes. In addition to the use of iodide ions as the shape controller, the authors also demonstrated that acetylacetonate precursors can alter the reduction kinetics of metal cations and thus control the one-pot synthesis of Pt-Pd hollow nanocubes. Compared to solid Pt-Pd nanocubes, the hollow Pt-Pd nanocubes with increased accessible surface area exhibited improved catalytic activity towards formic acid electrooxidation.

4.2.3 Seed-Mediated Growth

Morphological control of nanocrystals has become increasingly important, as many of their physical and chemical properties are highly shape-dependent. As a convenient and versatile synthesis method, seed-mediated growth is probably the most powerful route for the synthesis of bimetallic heterostructures with controlled morphology. In a seed-mediated growth process, a pre-synthesized seed of one metal is significant to serve as initial sites for the nucleation and growth of a second metal. During nucleation, the second metal can follow two different pathways by homogeneous and heterogeneous nucleation. Because the activation energy for nucleation on a pre-synthesized seed is prominently lower than that in a homogeneous nucleation process, the heterogeneous nucleation is always thermodynamically more favorable than homogeneous nucleation as long as the seed-mediated growth proceeds at a relatively slow rate under mild conditions, such as using weak reducing agent and at low temperature.

For seed-mediated growth, there are three major growth modes corresponding to the products with three distinct structures: (i) Frank-vander Merwe mode (or layer-by-layer growth) for core-shell nanocrystals, (ii) Volmer-Weber mode (or island growth) for hybrid structures, and (iii) Stranski-Krastanow mode (or island-on-wetting-layer growth) for branched structures [106]. According to the previously demonstrated results [107], the nucleation and growth mode of the second metal over the seed metal are mainly manipulated by various physical parameters, including lattice match, difference in bond dissociation energy and electronegativity between these two metals. As for Pt and Pd, due to the negligible lattice mismatch (only 0.77%) and the lack of galvanic replacement unless under the modified conditions (the presence of Br^-, I^- ions, etc.), the growth mode of Pd atoms on preformed Pt metal seeds (or Pt atoms on Pd seeds) is mainly determined by the bond dissociation energy.

Controllable synthesis of Pt-Pd bimetallic nanocrystals has been attracting increasing attention due to their novel catalytic properties which are distinctly different from those of their monometallic counterparts. Particularly, recent advances reveal that Pt-Pd bimetallic nanoelectrocatalysts with a core-shell structure have been recognized as a promising alternative to commercial catalysts for effectively improving the catalytic activity and durability for fuel cell application. To this end, a lot of studies have been performed to synthesize high-efficiency bimetallic Pt-Pd nanoelectrocatalysts with well-defined core-shell structures [108–115]. By manipulating the reaction kinetics, the growth and nucleation of Pt-Pd core-shell nanocrystals can be directed to a layer-by-layer epitaxial mode, leading to the formation of Pt-Pd core-shell nanocrystals. Yang and coworkers [116] developed a facile method for the synthesis of Pt-Pd core-shell cubes, cuboctahedra and octahedra through epitaxial growth of Pd on Pt cubic seeds. This process proceeded through reducing K_2PdCl_4 by ascorbic acid with Pt nanocubes (9.5 nm in edge length) as seeds and tetradecyltrimethylammonium bromide (TTAB) as a surfactant agent in an aqueous solution. Interestingly, in

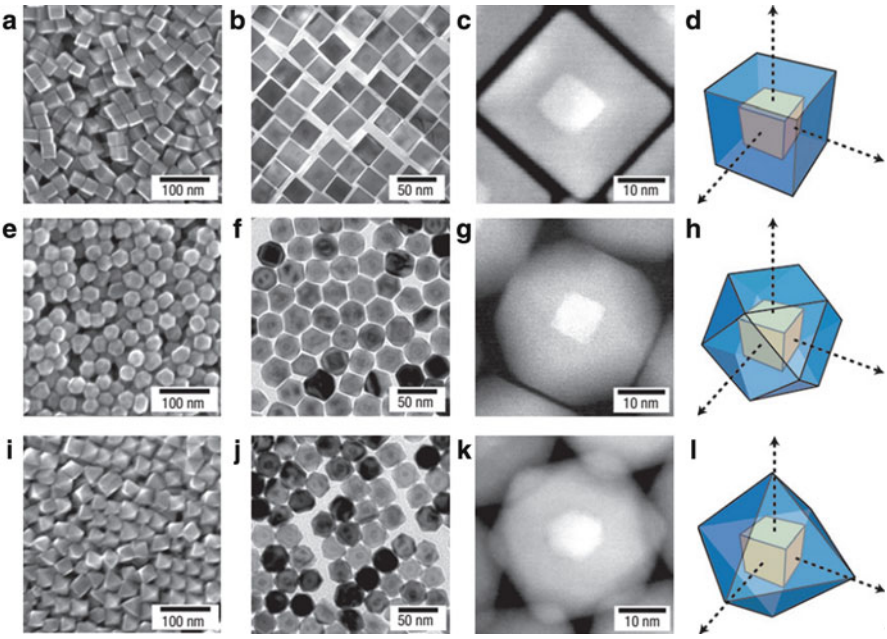

Fig. 4.7 SEM (the first column), TEM (the second column), HAADF-STEM (the third column) images of Pt-Pd core–shell nanocubes (**a**, **b**, **c**), cuboctahedra (**e**, **f**, **g**) and octahedral (**i**, **j**, **k**), and the modeled orientation (the fourth column) of the core and shell of Pt-Pd nanocubes (**d**), Pt-Pd cuboctahedra (**h**) and octahedral (**l**), respectively. Reprinted with permission from [116]. Copyright 2007 Nature Publishing Group

this synthesis, the authors found that by using different controlled facets of Pt cubic nanocrystals as nucleation centers for the overgrowth of Pd metal, shape-controlled Pt-Pd heterostructures can be obtained. The epitaxial growth of cubic Pd shells on cubic Pt seeds along the (100) and (111) directions resulted in the formation of Pt-Pd core-shell cubes. However, cuboctahedrally and octahedrally shaped Pd shells were formed upon addition of increasing amount of NO_2 which can alter the growth rates along the (100) and (111) directions to produce Pt-Pd core-shell cuboctahedron and octahedron. Both scanning electron microscopy (SEM) (Fig. 4.7a, e, i) and the corresponding transmission electron microscopy (TEM) (Fig. 4.7b, f, j) images clearly show the overall cubic, cuboctahedral and octahedral morphologies and monodispersity of the Pt-Pd products. Moreover, from the HAADF-STEM images, the Pt cores and the shaped Pd shells are discernible, demonstrating the layer-by-layer epitaxial growth on Pt nanocubes. As illustrated by the schematic drawings in Fig. 4.7d, h, l, the products evolved from Pt nanocubes to Pt-Pd cubes, cuboctahedra and octahedra along the (100) and (111) directions with different growth rates. This method and concept could also be used to synthesize other metal nanostructures such as FePt, CoPt, with desirable morphology.

In another study, Wang and coworkers [117] prepared Pt-Pd petal-like nanotubes via a wet-chemical strategy, in which the Pt nanotubes with petal-like surface was first synthesized using ultrathin Te nanowires as sacrificial templates and an effective epitaxial growth was further employed to deposit thin Pd nanoshells on the novel Pt nanotubes. It was found that the thickness of the Pd nanoshells can be easily controlled through the synthetic parameters (the amount of added Pd precursor, etc.). The obtained one-dimensional bimetallic Pt-Pd nanotubes with small diameter and nanometer-sized wall thickness demonstrated promising application in fuel cells as effective electrocatalysts.

Since Pt is extremely rare and expensive, it has been shown that deposition of Pt on Pd single-crystal surface can reduce the cost of materials while enhance their catalytic activity. By reducing H_2PtCl_6 with citric acid (CA) in the presence of Pd nanoplates as seeds and PVP as a stabilizing agent in an aqueous solution, Xia and coworkers synthesized Pd-Pt core-shell nanoplates with hexagonal and triangular shapes through layer-by-layer epitaxial growth of Pt on Pd nanoplates [118]. When AA was used instead of CA in this process, Pt-Pd nanodendrities rather than Pt-Pd core-shell structures were produced, indicating that the slow reduction rate associated with the weak reducing ability of CA played a vital role in achieving the epitaxial growth of Pt shells on Pd nanoplates. Furthermore, Pd-Pt core-shell structures with different shapes, such as regular octahedra, truncated octahedra and cubes, could also be obtained from the epitaxial growth of Pt on well-defined Pd nanocrystals [119]. The epitaxial growth of Pt shells on regular and truncated octahedra of Pd at slow reducing resulted in the formation of Pd-Pt core-shell octahedra. However, an incomplete octahedral Pt shell was formed when the Pd cube was used as a seed.

Most recently, by using rGO as a support, Bai et al. [120] developed a unique synthetic approach to prepare core-shell-like Pt-Pd-rGO stack structures. Two important steps (Fig. 4.8a) were suggested to be involved in the synthesis: (i) In situ growth of Pd nanocubes on rGO sheets via the co-reduction of K_2PdCl_4 and GO nanosheets by using ascorbic acid as a reducing agent, and (ii) Pt shells were coated onto the Pd nanocrystals by reducing H_2PtCl_6 in DMF. As shown in Fig. 4.8b, c, cubic nanocrystals with an average shell thickness of about 2 nm are dispersed on rGO sheets. HRTEM images in Fig. 4.8d show that the Pt shell is a single crystal enclosed by (100) facets, forming a perfect interface with the Pd nanocrystal. STEM and EDX mapping studies further confirm that Pt and Pd are enriched in the shells and cores, respectively. Importantly, the thickness of the Pt shell in the Pd-Pt-rGO stack structure can be controlled by simply changing the ratio of rGO-Pd to Pt precursors. Moreover, Pt can be selectively deposited on Pd nanocubes rather than on rGO sheets. In the synthesis of Pd-Pt-rGO structure, the potential difference of rGO and Pd causes the electrons accumulation on Pd surfaces, and then Pt can be preferentially reduced on the Pd surfaces with a relatively high electron density. Meanwhile, the more negative potential of rGO (0.38 V vs. SHE) than Pd (0.62 V vs. SHE) could provide a steady electron supply to prevent the oxidation of Pd in the redox reactions. All these results clearly demonstrate that rGO played a key role

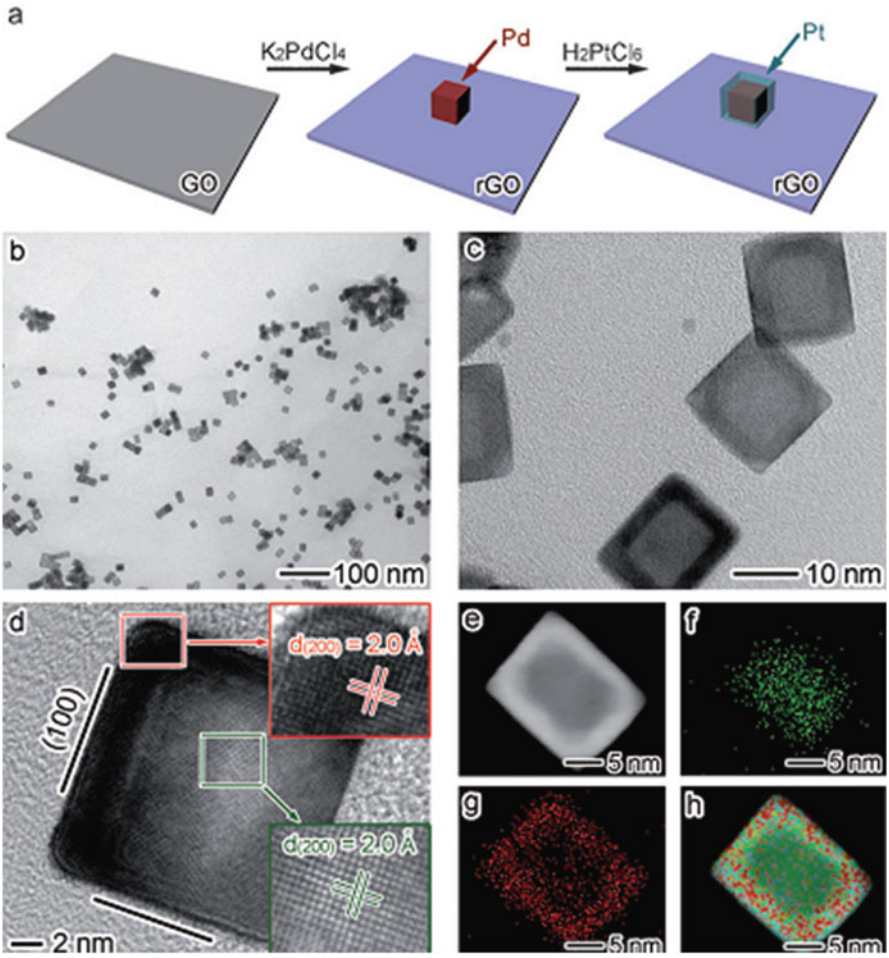

Fig. 4.8 (**a**) Schematic illustration of the synthesis of Pt-Pd-rGO structures. (**b**, **c**) TEM images of the Pt-Pd-rGO structure at different magnifications. (**d**) HRTEM image of a Pt-Pd nanocrystal supported on rGO. (**e**) STEM image and (**f**–**h**) EDS mapping profiles of a single Pt-Pd nanocrystal on rGO: (**f**) Pd (*green*), (**g**) Pt (*red*), and (**h**) Pt-Pd-STEM overlay. Reprinted with permission from [120]. Copyright 2014 Wiley-VCH

in manipulating the reaction kinetics to generate layer-by-layer epitaxial growth of Pt on Pd nanocrystals.

The layer-by-layer growth strategy was also extended to prepare Pt-Pd multi-shelled nanocrystals with alternating shells of Pt and Pd. Xia and coworkers [121] demonstrated a facile method for the heteroepitaxial growth of Pt-Pd nanocrystals with multi-shelled structures by sequentially adding Pt and Pd salt precursors into an aqueous solution containing Pt or Pd seeds with CA as both capping and reducing agents. Figure 4.9a shows a schematic of this synthesis starting from a

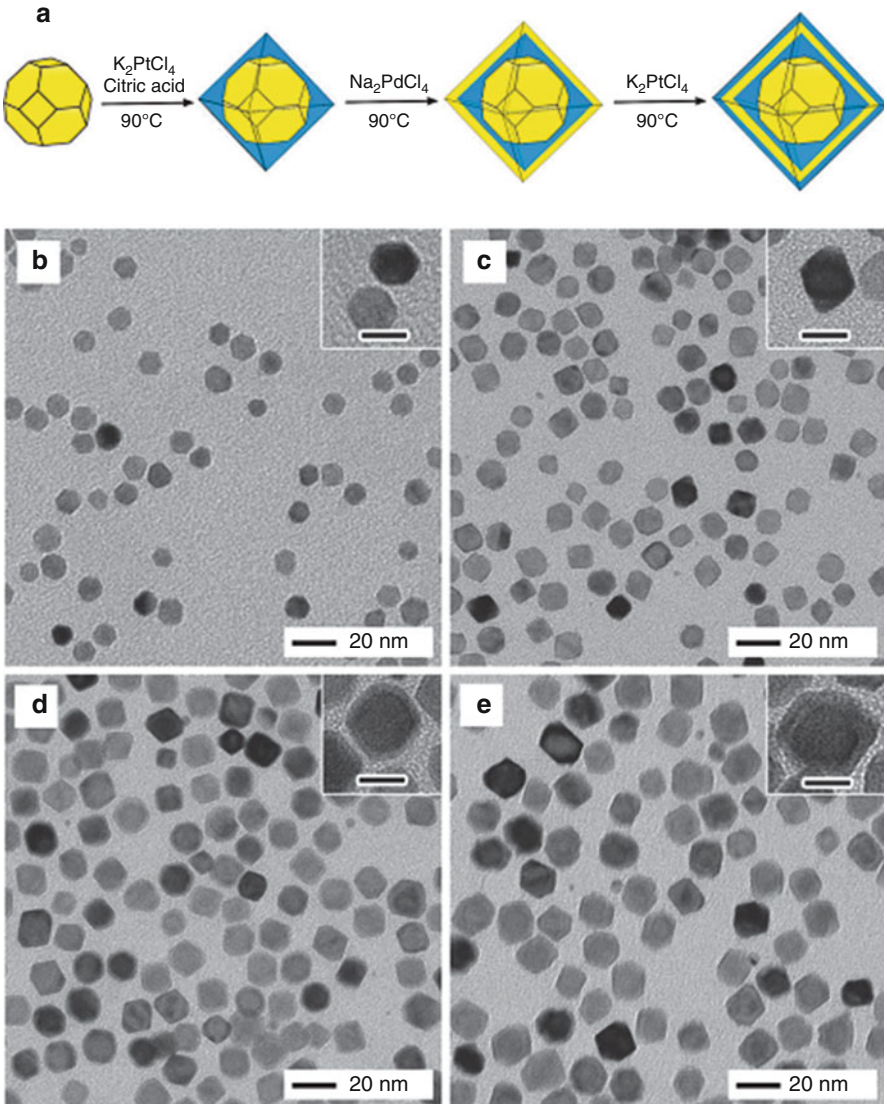

Fig. 4.9 (**a**) Schematic illustration of layer-by-layer epitaxial growth of Pt-Pd multi-shelled nanocrystals on a Pd cuboctahedral seed. (**b**) TEM image of Pd cuboctahedra of 9 nm in size that serve as seeds for the overgrowth steps. (**c**–**e**) TEM images of Pd@Pt (**c**), Pd@Pt@Pd (**d**), and Pd@Pt@Pd@Pt (**e**) nanocrystals prepared by reducing K_2PtCl_4 with citric acid (CA) as a reducing agent in the presence of cuboctahedral seeds of Pd. The insets show TEM images of individual nanocrystals at a higher magnification. Reprinted with permission from [121]. Copy right 2011 American Chemical Society

cuboctahedral Pd seed. The TEM images in Fig. 4.9b–e clearly shows a set of products obtained at different stages of this heteroepitaxial growth process, with the shape evolving from cuboctahedra to octahedra. The morphological transition

from cuboctahedra to octahedra derived from the preferential adsorption of CA on (1 1 1) facets of Pt, resulting in a faster growth rate along the Pt(1 0 0) direction than the (1 1 1) facets. The thickness of Pd and Pt shells could be independently manipulated by varying the amounts of Pd and Pt salt precursors added in the reaction solution. The core-shell nanocrystals with Pt and Pd shells can be repeated more times to generate larger and more complex Pd-Pt multi-shell nanocrystals. In addition to the use of Pd cuboctahedra as seeds for the alternating deposition of Pt and Pd shells, the authors found that Pd octahedra/plates and Pt cubes can also be employed as seeds to prepare Pt-Pd multi-shelled nanocrystals with other different shapes. For instance, starting from seeds of cubic Pt nanocrystals, Pt-Pd multi-shell nanocrystals composing of alternating Pd and Pt shells were also obtained, except for a morphological transition from cubes to octahedra owing to extensive overgrowth. All of these studies clearly demonstrated that the use of CA as both reducing and capping agents is the key to the successful synthesis of the multi-shelled nanocrystals. As a relatively weak reducing agent, CA can produce Pt and Pd atoms at the right place to ensure layer-by-layer epitaxial growth of both metals. The synthetic technique presented here can be used to prepare multi-shelled nanostructures with other compositions and morphologies for various applications.

Except for the afore-mentioned layer-by-layer growth mode, the island-on-wetting-layer mode is another preferred process for the growth of Pd on Pt seeds due to the following order in bond dissociation energy: $E_{\text{Pt-Pt}}$ (307 kJ/mol) > $E_{\text{Pt-Pd}}$ (191 kJ/mol) > $E_{\text{Pd-Pd}}$ (136 kJ/mol), resulting in the formation of Pt-Pd branched structures. Among various Pt-Pd heteronanostructures, Pt-on-Pd nanodendrites with highly branched shapes have received great interest because of their unique properties originating from the electronic coupling between the metals and a wide variety of promising applications in catalysis. Xia and coworkers [122] developed a facile, seed-mediated approach to the synthesis of Pt-Pd nanodendrites consisting of a dense array of Pt branches on a Pd nanocrystal core. In the synthesis, Pd truncated octahedra with an average size of 9 nm were used as seeds to direct the dendritic growth of Pt upon the reduction of K_2PtCl_4 by L-ascorbic acid (AA) in an aqueous solution containing PVP. It was proposed that the high initial supersaturation of Pt atoms associated with fast reduction by AA was probably responsible for the branched growth of Pt. In the reaction system, once Pt has nucleated on the surface of a Pd nanocrystal upon fast reduction by AA, the Pt nuclei can serve as catalytic sites for further reduction of the Pt precursor and create favorable sites for atomic addition. Growth preferentially occurs on the Pt nuclei, and deposition proceeds along the developing Pt branches. And the spatially separated Pt branches structures could be generated due to the multiple nucleation sites provided by truncated octahedral Pd seeds. The TEM images of the product showed that numerous Pt branches have grown from each Pd core, resulting in the formation of Pt-Pd nanodendrites. HRTEM characterizations clearly revealed the continuous lattice fringes from the Pd core to the Pt branches, further indicating the Pt branches were epitaxially nucleated and grown on the Pd seeds. The authors also found that the generated product has a high surface area and particularly active facets, providing a promising application in fuel cells. Furthermore, by using differently shaped Pd

seeds and mediated growth mechanism, other Pt-Pd dendritic nanostructures have also been generated [123, 124]. For example, Wang and coworkers [125] synthesized ultralong Pt-Pd bimetallic nanowires with a 100% yield by employing Pd nanowires as seeds to direct the dendritic growth of Pt upon the reduction of K_2PtCl_4 by AA in aqueous solution. Interestingly, the as-prepared Pt-Pd nanowires have the cores of Pd nanowires and shells of dendritic Pt, and the small single-crystal Pt nanobranches interweave with each other, resulting in nanopores on the surface of Pd nanowires. Due to the unique nanostructure, the synthesized Pt-Pd nanowires exhibited a high surface area and enhanced electrocatalytic activity towards methanol oxidation reaction.

In another study, Yang et al. [126] demonstrated an oil-phase synthetic approach for the synthesis of Pt-Pd branched nanostructures by reducing $Pt(acac)_2$ in a mixture of diphenyl ether and oleylamine with 5 nm Pd nanoparticles as seeds under an argon atmosphere at 180 °C. As shown in Fig. 4.10a, the branched arms of Pt with an average diameter of 3 nm are distributed evenly on the surface of Pd

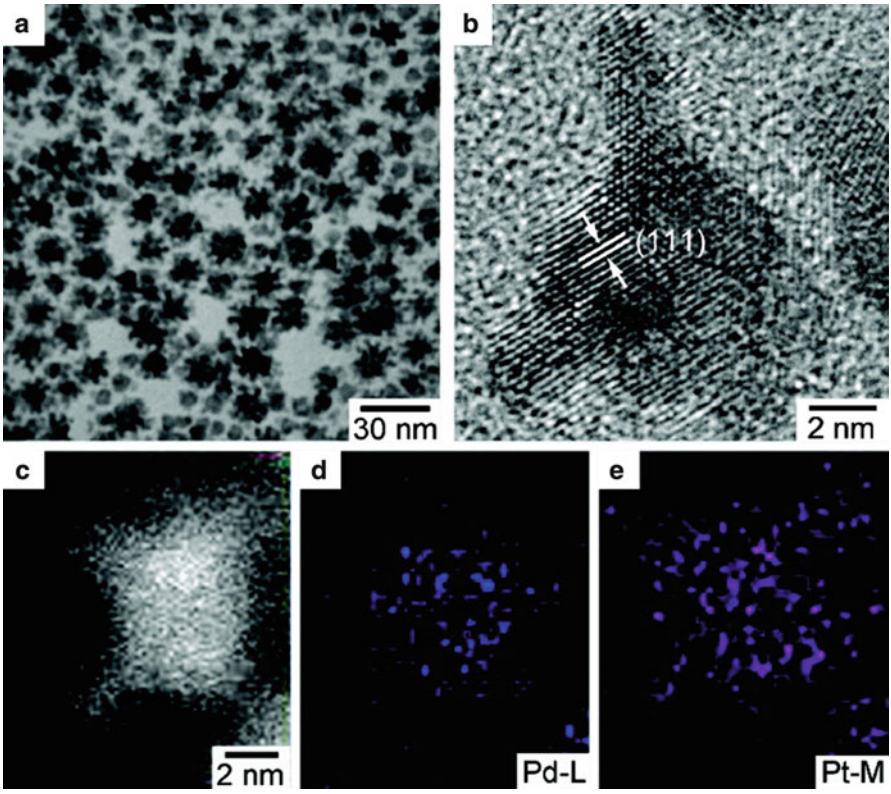

Fig. 4.10 Representative (**a**) TEM, (**b**) HRTEM (**c**) HAADF-STEM image and (**d**, **e**) EDX mapping of Pd-Pt bimetallic nanodendrites synthesized by reducing $Pt(acac)_2$ in a mixture of diphenyl ether and oleyamine in the presence of preformed Pd nanoparticles. Reprinted with permission from [126]. Copyright 2009 American Chemical Society

nanoparticles, generating Pt-Pd nanodendrite structures. From the HRTEM image (Fig. 4.10b), the synthesized nanoparticles show well-defined crystalline fringes and the Pt branches grew along the (1 1 1) crystal planes on the Pd seed. From the representative STEM and the corresponding EDX maps (Fig. 4.10c–e), Pt is dispersed throughout the entire particle, including the branches, whereas Pd could only be detected in the core region, indicating the formation of Pt-Pd dendritic structures.

Graphene nanosheets have been studied extensively owing to its unique electronic, thermal, mechanical properties arising from its strictly 2D structure. Particularly, its unique structure and the resulting properties endow it to be a promising 2D supporting material to load metal nanoparticles for application in fuel cells. By using graphene sheets as support, Wang and coworkers [127] constructed high-quality 3D Pt-on-Pd bimetallic nanodendrites supported on PVP-functionalized graphene nanosheets. In the synthetic process, the PVP-functionalized graphene was first obtained under the reduction of hydrazine. Pd/graphene seeds were then synthesized using HCOOH as reducing agent at room temperature. Finally, Pt-on-Pd nanodendrites supported on graphene sheets were produced by using graphene sheets-supported Pd nanoparticles as seeds to direct the dendritic growth of Pt upon the reduction of K_2PtCl_4 by ascorbic acid in an aqueous solution. The TEM results indicated that the Pt-on-Pd bimetallic nanodendrites with an average size of 15 nm were dispersed on graphene sheets, in which Pt branches with an average diameter of about 3–5 nm were distributed evenly on the surface of a Pd nanoparticle. Importantly, the number of Pt branches could be easily controlled through simply manipulating the reaction parameters. For example, lower concentrations of graphene can lead to relatively lower amounts of Pd nanoparticles adsorbed on the surface of graphene nanosheets, thus resulting in Pt-on-Pd bimetallic nanodentrites with more Pt branches supported on the graphene sheets. More importantly, because the small single-crystal Pt nanobranches with porous structure and good dispersion were directly grown onto the surface of graphene nanosheets, the obtained hybrids exhibited an enlarged electrochemical surface area as high as 81.6 m^2/g. All these unique structural features together with the synergetic effects of the Pt-Pd and the enhanced electron transfer stemming from graphene support are highly favorable for the application of the graphene nanosheets-supported 3D Pt-on-Pd bimetallic nanodendrites in fuel cells, with a much higher catalytic activity than conventional E-TEK Pt/C electrocatalysts for methanol electro-oxidation.

In spite of the significant achievement in the synthesis of Pt-on-Pd nanodendritic structures *via* the aforementioned seed-mediated growth strategy, the involved processes of the syntheses were strongly dependent on the use of faceted Pd seeds to direct the subsequent growth of Pt branches. Without the well-defined Pd seeds, both the particle size and shape of the Pt-on-Pd nanodendrites are usually uncontrollable. Recently, without using any pre-synthesized Pd seeds, organic solvent and high temperature, Wang et al. [128] proposed a simple approach for one-step direct synthesis of Pt-on-Pd nanodendrites in aqueous solution at room temperature. In the synthesis, a block copolymer (Pluronic P123) was employed to

mediate the reduction of K_2PtCl_4 and Na_2PdCl_4 by using AA as a reducing agent for 30 min at room temperature. It was found that the as-prepared product consists of well-dispersed nanodendrites with Pd interior and dendritic Pt exterior, in which the Pt nanoarms have widths of 3 nm branching in various directions. The preferential reduction of the Pd precursor by AA caused by the different reduction kinetics of Pd and Pt complex with AA was found to a key factor in directing the formation of Pt-on-Pd nanodendrites. The formed Pd nanoparticles can serve as in situ seeds for the subsequent deposition of Pt. Moreover, the use of Pluronic P123 and the selected concentration (0.87 mM) also played critical roles in the synthesis of Pt-on-Pd nanodendrites. In comparison, aggregated Pt-Pd nanoclusters were obtained with an increase/decrease of the Pluronic P123 concentration or replacing Pluronic P123 with Pluronic F68. A surfactant of PVP was found to be unfavorable for the formation of Pt-on-Pd nanodendrites. Most importantly, by a simple control of the mole ratios of the Pt and Pd precursors in the reaction solution, Pt-on-Pd nanodendrites with a designed Pt and Pd content could be obtained. In comparison with the two-step seed-mediated methods, this rational block copolymer-mediated synthesis could trigger the facile creation of novel bimetallic heterostructures with designed compositions and desired properties.

In addition to seed-mediated growth involving direct reduction of a second metal onto pre-formed seeds, Beer and co-workers [129] recently reported a novel anion coordination route to control the formation of bimetallic core-shell nanoparticles for any two noble-metals including Pt and Pd. This method uses ligand-based supramolecular forces to ensure surface segregation of the shell metal onto the pre-formed core before its reduction. And four different types of bimetallic core-shell nanoparticles (Au-Pd, Pd-Au, Pt-Pd and Pd-Pt) with an average size of less than 5 nm have been synthesized by using this new protocol. The success of this synthesis was based on the ability to anchor metal ions to the pre-formed seeds through amides-chlorometallates anion coordination by hydrogen bonding before reduction occurred. This work not only provides novel core-shell nanoparticles with small size (<5 nm), but also offers an impetus for the exploitation of supramolecular interactions in the design and synthesis of structured nanoparticles with controlled composition.

4.2.4 Electrochemical Deposition and Its Combination with Galvanic Replacement

In recent years, to improve the mass activity of shaped nanocrystals, much work has focused on the crystallographic orientation of metal atoms at the surface of nanocrystals [30, 130]. Owing to the simplicity and no need of templates, electrochemical deposition is a useful approach to prepare Pt-Pd bimetallic nanocrystals with decorated surface by Pt or Pd adatoms and consequently with enhanced electrochemical properties [131–144]. For example, Feliu and coworkers [145]

have successfully electrodeposited Pd adatom on cubic Pt nanoparticles as an anode electrocatalyst toward formic acid oxidation in fuel cells. The authors proposed that the amounts of Pd on the Pt surfaces can be easily monitored in situ by observing the voltammetric changes during the deposition process. Compared with the Pd-modified quasispherical Pt nanoparticle, the Pd adatoms-decorated Pt(100) nanoparticles exhibited enhanced catalytic activity for formic acid electrooxidation. In the Pd adatoms-decorated Pt(100) nanoparticles, the high fraction of Pt(100) sites can decrease surface poising, lower onset potential and thus greatly improve the kinetics of formic acid oxidation over Pt surface.

In addition, the nanostructure of Pd nanocrystals covered by a Pt monolayer shell has also attracted much attention because in such structure all Pt atoms located on the surface of Pd core can be sufficiently utilized and thus improved Pt mass activity can be achieved. DFT calculations demonstrated that the strong interaction between the Pt monolayer and the base metal also plays a vital role in determining the structure and properties of the Pt monolayer. In this case, the electrocatalytic properties of the Pt monolayer can be easily manipulated by changing the base metal. For example, the electrocatalytic activity of a Pt monolayer on different base metals for ORR exhibited a volcano-type dependence [146]. Pd substrate was thought not only to apply a compressive strain upon the Pt monolayer but also to impart a so-called "ligand-effect", leading to lowered energy of the weighted center of the Pt d-band. Therefore, the Pd(111) decorated with Pt monolayer is located at the top of the volcano curve with the highest ORR activity. The extremely low Pt loading together with a perfect catalytic activity make the Pt-monolayer decorated Pd nanocrystals very attractive for practical applications in fuel cells.

Recently, much work has been done to prepare Pt monolayer-decorated Pd nanocrystals with improved electrocatalytic properties [147–150]. For example, Adzic and coworkers [151] reported a simple approach for the synthesis of a Pt monolayer on a Pd base metal by first electrochemically depositing a monolayer of Cu atoms on Pd cores through Cu underpotential deposition (UPD), followed by the controlled displacement of these adatoms with Pt *via* galvanic exchange. Figure 4.11a schematically illustrates the key steps for the growth of a Pt monolayer on a Pd core. The Z-contrast image from HAADF-STEM (Fig. 4.11b) demonstrates the formation of a bright shell on the relatively darker nanoparticle core. The EDX line-scan analysis (Fig. 4.11c) shows that the Pt trace has two peaks in two sides, while the Pd trace has one peak in the center, further confirming the formation of a Pt monolayer on the Pd core. In addition, the thickness of the Pt shell could be gradually increased with repeated UPD and galvanic replacement processes.

Although outstanding ORR activities have been achieved with the aforementioned 0D core-shell catalysts, 1D nanostructures are characterized by their uniquely anisotropic nature, which imparts advantageous structural and electronic factors in the catalytic reduction of oxygen. In particular, Koenigsmann et al. [152] designed a Pd nanowire core-Pt monolayer shell structure with enhanced electrocatalytic activity and durability by successfully combining the uniquely advantageous core-shell motif with the electrocatalytic advantages of ultrathin 1D nanostuctures. In their synthesis, the ultrathin Pd nanowires (~2 nm) were first

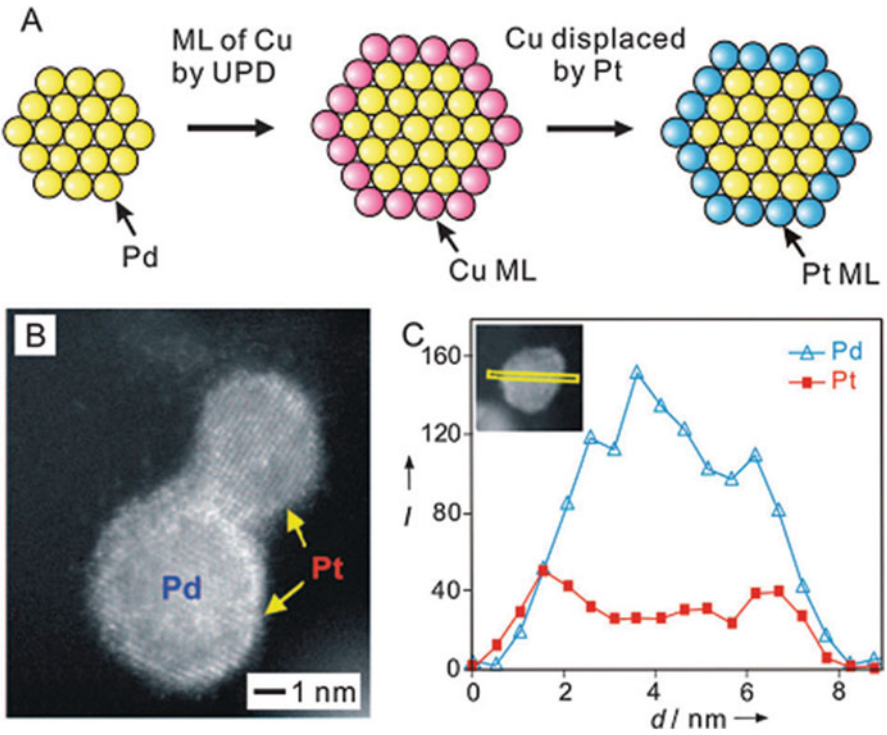

Fig. 4.11 (**a**) A schematic of the two major steps involved in the synthesis of a Pt monolayer on a Pd core through a combination of electrochemical deposition and galvanic replacement. (**b**) HAADF-STEM image and (**c**) the EDX line-scanning profile showing the formation of a Pt monolayer on a Pd nanoparticle. Reprinted with permission from [151]. Copyright 2010 Wiley-VCH

synthesized, and the deposition of Pt onto the surface of the treated Pd nanowires was achieved by Cu UPD followed by galvanic displacement of the Cu adatoms with Pt^{2+}. Importantly, the use of ultrathin nanowires with a diameter below 5 nm in this work could maximize the surface area-to-volume ratio, achieving higher mass activity compared with conventional commercial Pt nanoparticles, and core-shell nanoparticles. Moreover, in the obtained Pd nanowire core-Pt monolayer shell structure, a contraction of the core nanowire surface would be highly advantageous for ORR electrocatalysis, because this would enhance the strain-induced contraction of the Pt monolayer and therefore improve the inherent ORR activity. In addition, by varying the shape of the Pd cores (Pd cubes, octahedra or rods), the morphology-tailored core-shell nanoparticles could also be obtained by the same way [150, 153, 154].

In addition to the methods listed above, the synthesis of Pt-Pd (or supported Pt-Pd) bimetallic nanocrystals can also be achieved by other techniques, such as thermal treatment [155–160], plasma sputtering [161, 162], electroless deposition [163, 164], and supercritical CO_2 deposition [165, 166].

4.3 Applications of Unsupported/Supported Pt-Pd Bimetallic Nanocrystals as Electrocatalysts in Fuel Cells

4.3.1 Alcohol Oxidation Reaction

Among the various fuel cell technologies, direct methanol fuel cells (DMFCs) have attracted special interests because of their ability to utilize methanol as a liquid fuel, which can be easily and safely stored as well as transport comparing with hydrogen-based counterparts [167, 168]. Moreover, methanol can be directly prepared either from natural gas or renewable biomass and thus ideally meet the future power needs with a high energy efficiency of 600 Wh/kg [169]. More importantly, DMFCs have the unique advantage of operation at near ambient temperatures between 40 and 80 °C, which is much lower than the normal operating temperatures for solid oxide fuel cells (800–1000 °C). Therefore, DMFCs technology represents a potentially effective fuel cell candidate for future applications in the automotive, portable power generating, and electronics industries [170]. However, it is significant to note that large portions of the cost of DMFCs can be attributed to the high loading of expensive electrocatalysts that are at the heart of the device itself. Meanwhile, the slow anode reaction and methanol crossover reaction at the cathode are also the vital limitation to the widespread application of DMFCs. Hence, lowering the costs and improving efficiency of the catalysts have become two critical technological issues towards the development of practical and inexpensive DMFCs.

The process of methanol oxidation reaction (MOR) at the anode in DMFCs includes the methanol adsorption and the subsequent dissociation into adsorbed intermediates [171]. According to the dual-pathway mechanism, CO is a poisoning intermediate species, which can largely reduce the catalytic activity of catalysts, especially Pt-based catalysts. To eliminate the CO poisoning to catalysts, oxygen-containing surface species (e.g, OH) formed on adjacent catalyst sites are usually needed to remove CO adsorbed on the catalyst surface (CO_{ad}). Thus, to catalyze the methanol oxidation efficiently, catalysts with multiple active sites are required for the adsorption of methanol and formation of OH species. Therefore, a significant amount of work has been dedicated to the synthesis of Pt-based nanostructures combining with another metal so as to improve CO-tolerance. Among these, Pt-Pd bimetallic nanocrystals represent an active and durable catalysts for methanol oxidation.

Effectively controlling the size and shape of Pt-Pd bimetallic nanocrystals can provide a great opportunity to improve their catalytic properties and increase their mass or specific activity [57, 100, 110]. Huang and coworkers [115] employed a seed-mediated growth method to synthesize Pt-Pd core-shell nanocrystals with different Pd shell thicknesses. The catalytic activities of the different sizes (i.e. Pd shell thickness) of Pt-Pd nanocrystals at Pd/Pt ratios from 1/6 to 2/3 for MOR in alkaline media were compared in CV measurements. It was found that the Pt-Pd core-shell nanocrystals with a Pd/Pt ratio of 1/3 (near monolayer Pd shell)

yield the highest current density and the most negative potential for the oxidation peak in the forward sweep due to the highest tolerance of the sample to CO poisoning. Such results demonstrate the importance of Pd shell thickness of the core-shell nanocrystals in the manipulation of the catalytic performance for fuel cell applications.

To enhance the mass activity of Pt, the core-shell type of nanocrystal catalysts with a Pt shell have also been developed to remarkably reduce Pt loading. Yamauchi and coworkers [128] synthesized Pt-on-Pd nanodendrites and studied their catalytic properties for methanol oxidation reaction in acid condition. The electrochemical measurements showed that the forward peak current density of MOR on Pt-on-Pd (0.49 A/mg_{Pt}) is much higher than that of Pt nanodendrites (0.21 A/mg_{Pt}) and Pt black (0.11 A/mg_{Pt}), and at any oxidation current density, the corresponding oxidation potentials on the Pt-on-Pd nanodendrites are obviously lower than those on the Pt dendrites and Pt black, indicating that Pt-on-Pd nanodendrites has the highest activity for methanol oxidation. It was found that the formation of the inserted pseudo-Pd-Pt alloy heterointerface plays a critical role in reducing the electronic binding energy in Pt and facilitating the C-H cleavage reaction in methanol decomposition. Furthermore, the various atomic steps exposed on the Pt branch surface can act as highly active sites for the methanol oxidation reaction. Therefore, superior catalytic activity was exhibited through this open dendritic structure with the designed Pt and Pd ratios. In addition, nanostructures with high aspect ratios such as nanowires, nanotubes and nanorods can provide improved mass transport and higher electrochemical active surface area than those of low aspect-ratio nanoparticles [172]. For example, Guo et al. [125]. investigated the activity of the ultralong Pt-Pd bimetallic nanowires for methanol oxidation reaction. By comparing with other catalysts, the Pt-Pd nanowires exhibited much larger electrochemical surface area (ECSA) (90.7 m^2/g) than those of E-TEK Pt/C catalyst (53.5 m^2/g) and mesoporous Pt with giant mesocages (74 m^2/g). Compared to the commercial E-TEK catalyst, a significant enhancement of the peak current and a negative shift of the onset potential of methanol oxidation were achieved on the Pt-Pd nanowires. Moreover, it should be noted that the Pt-Pd nanowires also exhibited much higher mass activity and stability than some state-of-art Pt-based nanomaterials.

It has been well-documented that the catalytic activities of bimetallic nanocrystals are strongly dependent on their compositions [139, 173]. Sun and co-workers [89] studied polyhedral Pt-Pd bimetallic nanoparticles with the compositions ranging from $Pd_{88}Pt_{12}$ to $Pd_{34}Pt_{66}$ as anode catalysts for methanol oxidation reaction. As shown in Fig. 4.12a, as compared to pure Pd nanoparticles, both peak potentials and current densities of MOR change with the Pt content in the Pt-Pd nanoparticles. The plots of peak potentials and peak current densities versus Pt atomic % in the nanoparticles (Fig. 4.12b) showed a composition-dependent MOR activity and the catalyst having 40–60% Pt exhibited the maximum activity plateau. Cai and coworkers [82] synthesized three-dimensional Pt-Pd core-shell nanostructures by using a one-step microwave heating method. It was found that the Pt-Pd nanostructure with a Pd/Pt molar ratio of 1:3 exhibited the highest

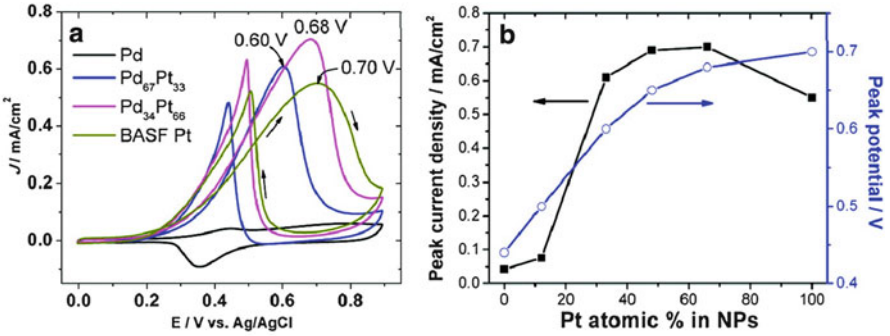

Fig. 4.12 (**a**) J-V curves of MOR on Pd, BASF Pt and Pd-Pt catalysts with different compositions in 0.1 M $HClO_4$ and 0.1 M methanol. (**b**) Methanol oxidation peak current density and peak potential vs the Pt atomic % in the Pt-Pd nanoparticles. Reprinted with permission from [89]. Copyright 2011 American Chemical Society

electrocatalytic activity toward methanol oxidation as compared to Pt, Pd and other Pt-Pd nanostructures. Moreover, the Pt-Pd nanostructure with a Pd/Pt molar ratio of 1:3 also exhibited high stability due to its enhanced tolerance to intermediate species during the methanol oxidation. Jin and coworkers [88] investigated the catalytic activity of the assembled free-standing Pt-Pd nanomembranes (PdPt-FNMs) for methanol oxidation in alkaline condition. By using the hydrogen adsorption-desorption method, the PdPt-FNMs have much higher ECSA values ($Pd_{53}Pt_{47}$–FNMs (48.01 m^2/g), $Pd_{33}Pt_{67}$–FNMs (52.04 m^2/g), $Pd_{15}Pt_{85}$–FNMs (50.55 m^2/g)) than commercial Pt black (22.94 m^2/g), indicating the enhanced active sites on PdPt–FNMs for the electrooxidation of methanol. By comparing the CVs of methanol oxidation, the $Pd_{33}Pt_{67}$–FNMs exhibited the best catalytic performance with the most negative onset potential and the largest current density among the PdPt-FNMs with different compositions and commercial Pt black. Moreover, the PtPd-FNMs showed higher stability than commercial Pt black after CV cycling tests, and the $Pd_{33}Pt_{67}$–FNMs exhibited the highest stability with the least loss of the electrocatalytic activity among the studied PdPt-FNMs. The enhanced MOR activity of all the above-mentioned Pt-Pd bimetallic nanocrystals can be explained by the bifunctional methanol oxidation mechanism. In the Pt-Pd nanocrystals, Pd is mainly responsible for the water dehydrogenation to form Pd-OH, while Pt catalyzes the methanol dehydrogenation to form Pt-CO. The reaction between Pd-OH and Pt-CO produces CO_2 to regain the active metal surfaces. However, without Pd, the water dehydrogenation on Pt occurs at a higher potential, making the oxidation process sluggish. The activity also decreases with the excessive Pd due to the lack of Pt for methanol dehydrogenation.

In the synthesis, metal nanoparticles are usually formed with certain facets to minimize surface energy and the total free energy. On different crystal surfaces of Pt-Pd materials, the electronic structures and atomic arrangements are quite different, and the appropriate crystal phase is able to greatly enhance reaction kinetics

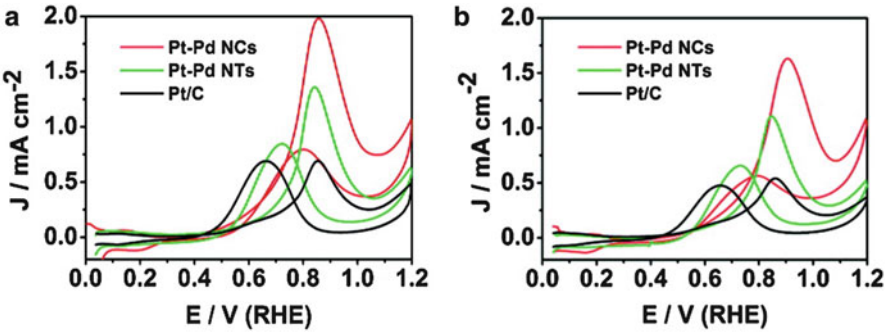

Fig. 4.13 (**a**) Stable CV curves obtained from the Pt-Pd NCs, NTs, and Pt/C in 0.1 M $HClO_4$ and 1 M CH_3OH at a sweep rate of 50 mV/s. (**b**) CV curves obtained from different electrocatalysts after 4000 additional cycles. Reprinted with permission from [94]. Copyright 2011 American Chemical Society

[113]. Yin et al. [94] have successfully prepared the mono-disperse single-crystalline sub-10 nm Pt-Pd nanotetrahedra (NTs) and nanocubes (NCs). The single-crystalline Pt-Pd NTs are enclosed by four (1 1 1) facets, while the Pt-Pd NCs are enclosed by (1 0 0) facets. As shown in Fig. 4.13a, both the Pt-Pd NCs and NTs exhibited high catalytic activities towards methanol electrooxidation in acid electrolyte. As compared the peak voltage ($E_f = 0.85$ V) and the peak current density ($J_f = 0.51$ mA/cm^2) for Pt/C, more negative E_f and much larger J_f in a forward scan were obtained with 0.85 V and 1.49 mA/cm^2 for Pt-Pd NCs, and with 0.84 V and 1.12 mA/cm^2 for Pt-Pd NTs, respectively. Moreover, the ratio of the current density values in two sequential forward (positive) and backward (negative) sweeps (J_f/J_b) is considered to be an important indicator of the catalyst tolerance to poisoning species. The different J_f/J_b values for Pt-Pd NCs (2.5) and NTs (1.4) confirmed that different reaction pathways might be adopted on the (1 0 0) or (1 1 1) surfaces. Meanwhile, due to the more durable nature of the (1 1 1) facet of Pt-based nanocrystals, the Pt-Pd NTs remained higher activities than both Pt-Pd NCs and Pt/C after repeating the CV sweeps for over 4000 cycles (Fig. 4.13b). The different electrocatalytic performances of the Pt-Pd NCs and NTs demonstrate the facet-sensitive nature of methanol oxidation on Pt-Pd nanocrystals.

In another study, Lee et al. [72] synthesized octahedral Pt-Pd nanoparticles with exposed (1 1 1) facets as anode catalysts for methanol oxidation. The octahedral Pt-Pd alloy with dominantly exposed (1 1 1) facets exhibited an enhanced catalytic performance with lower onset and peak potentials, and higher current density as compared to polycrystalline Pt/C for MOR. Moreover, a higher ratio of the forward to the reverse anodic peak current density than that of commercial Pt/C indicates less accumulation of residues on the Pt-Pd octahedron during the forward anodic scan. In addition, the remained size and morphology of the well-defined Pt-Pd alloy octahedron compared to the massive agglomeration of Pt/C after the stability test further confirmed the superior electrocatalytic activity and stability of the Pt-Pd bimetallic nanocrystals for MOR. All these studies indicate that shape-controlled

synthesis of facet-sensitive multi-metal nanocrystals can open up new opportunities for Pt-Pd nanocrystals with potential applications.

To further improve the catalytic activity of the Pt-Pd bimetallic nanocrystals and lower the usage of noble metals, loading of catalysts on the surface of suitable supporting materials is highly desirable [43, 54, 81, 96, 174, 175]. Wang and coworkers [127] investigated the catalytic activity of three-dimensional Pt-on-Pd bimetallic nanodendrites supported on graphene nanosheets (TP-BNGN). By comparing with the carbon nanofiber- or CNT-supported Pt nanoparticles, CNT/Pt composite and commercial E-TEK Pt/C catalysts, the TP-BNGN exhibited much improved catalytic activity for MOR with much higher mass current density, more negative onset oxidation potential and more efficient removal of the poisoning species on the catalyst surface. Recently, we studied the catalytic activities of rGO-supported Pt-Pd nanocubes (PtPd/rGO) for methanol oxidation in acid medium [95]. As shown in Fig. 4.14, compared with the unsupported PtPd alloy nanocubes and commercial Pt/C catalysts, the PtPd/rGO showed enhanced

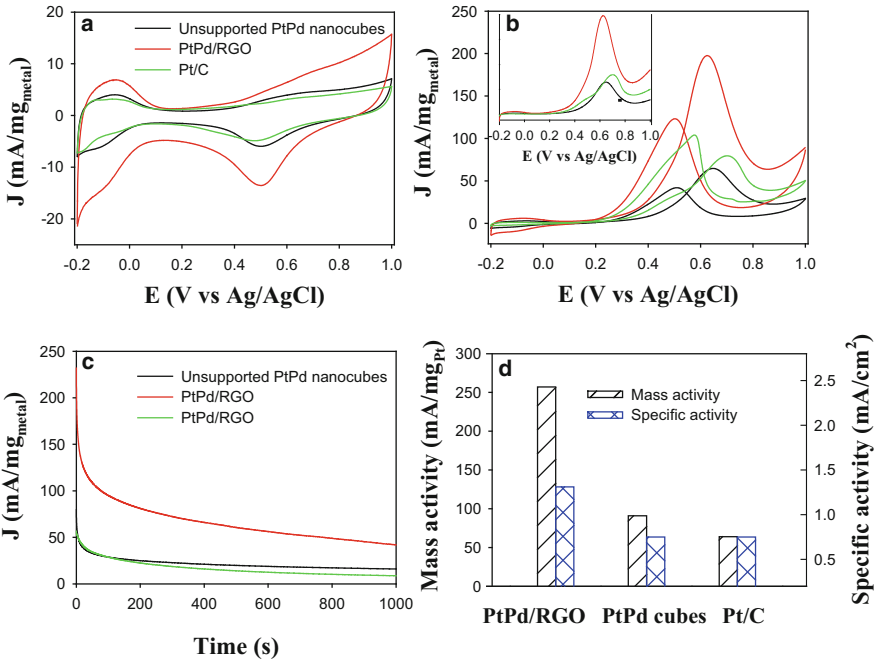

Fig. 4.14 CVs of the unsupported and rGO-supported (PtPd/rGO) PtPd alloy nanocubes, and the commercial Pt/C catalysts in (**a**) 0.1 M $HClO_4$ solution, and (**b**) 0.1 M $HClO_4$+1.0 M CH_3OH solution. (**c**) Chronoamperometric curves of methanol oxidation at 0.62 V in 0.1 M $HClO_4$+1.0 M CH_3OH solution after the CO stripping treatment. Potential scan rate 50 mV/s. All currents were normalized to the total mass of noble metals (Pt and Pd). (**d**) Comparison of mass and specific activities of the three catalysts for methanol oxidation. Reprinted with permission from [95]. Copyright 2013 American Chemical Society

electrocatalytic performance with increased ECSA, lower negative onset potential and higher current density for methanol oxidation. Furthermore, the PtPd/rGO exhibited high durability during the methanol oxidation. All these studies indicate that graphene sheets can be used as excellent catalyst support for enhancing the catalytic performance and improving the stability of Pt-Pd bimetallic catalysts.

With a high surface area, good electrical conductivity, light weight, high chemical stability and inherent size and hollow geometry, carbon nanotubes (CNTs) are one of the most attractive nanomaterials used as an efficient catalyst support in fuel cells. Wai and coworkers [166] studied the catalytic activity of Pt-Pd nanoparticles supported on multi-walled carbon nanotubes (MWCNT) for methanol electrooxidation. From the CVs of methanol oxidation, compared to MWCNT-supported monometallic nanoparticles, the Pt-Pd/MWCNTs exhibited much lower onset potential and higher ratio of the forward scan peak current over the backward scan peak current, indicating the Pt-Pd/MWCNTs catalysts are more efficient at lowering the adsorbed carbon monoxide and thus show an enhanced catalytic activity for MOR.

In addition, conducting polymer nanostructures have recently received special attention as supporting nanomaterials owing to their highly π-conjugated polymeric chains, unique electrical properties, and controlled morphologies. Recently, Wang and coworkers [76] reported a 1D nanoelectrocatalyst based on polyaniline (PANI) nanofiber-supported Pt-Pd hybrid nanoparticles for methanol oxidation reaction. From the CV measurements, the current density of MOR on the PANI nanofiber-supported Pt-Pd nanoparticles catalyst was 2.99 times higher than that of E-TEK Pt/C catalyst for MOR. And the hybrid catalyst exhibited a higher ratio (1.98) of the forward oxidation current peak to the reverse current peak compared to commercial E-TEK Pt/C (1.08), revealing the more effective removal of the poisoning species on the surface of PANI nanofiber-supported Pt-Pd nanoparticles. The enhanced catalytic activity of PANI nanofiber-supported Pt-Pd can be ascribed to the high conductivity of PANI support in acidic conditions and the supra-high density distribution of small Pt-Pd nanoparticles on the surface of PANI nanofibers. In another work, highly dispersed Pt-Pd nanoparticles supported on polypyrrole (Ppy) film were fabricated by electrochemical deposition method [137]. Because of the uniform dispersion of Pt-Pd nanoparticles in the Ppy film, the synergistic effect of the Pt and Pd and the effective reduction of CO species, the Ppy-supported Pt-Pd nanoparticles showed remarkably improved electrocatalytic performance for methanol oxidation reaction. Galal et al. [140] synthesized Pt-Pd nanoparticles supported on poly(3-methylthiophene) (PMT) films via electro-deposition method. The voltammetric measurements indicated a higher activity of PMT-supported Pt-Pd nanoparticles than other types of deposited substrates such as Pt and glassy carbon, for methanol oxidation. Moreover, it was also found that the thickness of PTM in the Pt-Pd/PTM hybrid has an obvious effect on the catalytic performance, and the best activity was obtained at the relatively thinner films.

Direct ethanol fuel cells (DEFCs) have also attracted enormous attention due to the higher theoretical energy density but less toxicity of ethanol as compared to methanol. Moreover, ethanol can be synthesized directly from biomass, whereas

methanol is most commonly generated from natural gas, an abundant but non-renewable source [176]. For ethanol oxidation on Pt-based electrocatalysts, several reaction mechanisms have been proposed with complex processes [177, 178]. According to the mechanisms, it is widely accepted that the electro-oxidation of ethanol can only occur with a multifunctional electrocatalyst. Platinum itself is known to be rapidly poisoned on its surface by strongly adsorbed species coming from the dissociative adsorption of the ethanol molecule. So other metals modified with Pt can activate water at low potentials to produce oxygenated species (e.g. adsorbed OH), and these OH species are necessary to oxidize the species from the dissociation of ethanol to carbon dioxide. Moreover, unlike methanol oxidation, the oxidation of ethanol is more difficult with the necessity to break the C-C bond to obtain its complete oxidation. Except for the formation of adsorbed CO, acetaldehyde, acetic acid, or CO_2 can be formed through different reaction pathways during ethanol electro-oxidation reaction. In the past years, Pt-Pd bimetallic nanocrystals have been recognized as a promising alternative to commercial catalysts for effectively improving the activity and durability for ethanol electro-oxidation [64, 142, 155]. For example, Guo et al. [117] synthesized Pt-Pd bimetallic nanotubes with petal-like surface and further studied their catalytic activity for ethanol oxidation in alkaline media. Figure 4.15a compares the CVs of Pt-Pd bimetallic nanotubes with petal-like surfaces (PBNPSs, curve a), Pt nanotubes with petal-like surfaces (PNPSs, curve b) and E-TEK Pd/C (curve c) electrodes in a N_2-saturated 0.5 M H_2SO_4 solution. It can be seen that the reduction peak potential of $Pd(OH)_2$ shifts positively on the PBPNSs (0.48 V vs. Ag/AgCl) as compared with E-TEK Pd/C (0.38 V vs. Ag/AgCl), indicating the reduced oxophilicity and weakened chemisorpotion with oxygen-containing species on PBNPSs catalyst. Furthermore, from the CVs of ethanol oxidation shown in Fig. 4.15b (specific activity), c (mass activity), the PBNPSs (curve a) exhibit much higher specific and mass activities, which are about 3.7 and 3.1 times larger than PNPSs (curve b), demonstrating the importance of thin Pd shells for enhancing ethanol electro-oxidation. Meanwhile, from Fig. 4.15b, c, the PBNPSs also show higher specific (3.05 times) and mass (3.7 times) activities than the E-TEK Pd/C catalyst. In addition, after 1800 s continuous operating (Fig. 4.15d), the specific activities of PBNPSs (curve a) are much higher than those of the PNPSs (curve b) and commercial Pd/C (curve c), suggesting that the PBNPSs catalyst has great stability in ethanol oxidation reaction.

Recently, Lee and co-workers [144] prepared bimetallic Pt-Pd alloy nanoparticles on a Nafion-graphene film by a simple electrochemical deposition method. Due to the synergistic effects of the PtPd nanoparticles and the enhanced electron transfer originating from graphene, the hybrid exhibited efficient catalytic activity and stability toward ethanol electro-oxidation in alkaline media. Datta et al. [49] successfully incorporated Pt-Pd bimetallic nanocrystallites into polyvinyl carbazole (PNVC) cross-linked with V_2O_5 (PNVC-V_2O_5) and investigated its electrocatalytic activity for ethanol oxidation in alkaline condition. As compared to the Pt/C, PtPd/C and Pt/PNVC-V_2O_5, the PtPd/PNVC-V_2O_5 catalyst exhibited enhanced electrocatalytic performance with increased electrochemical active

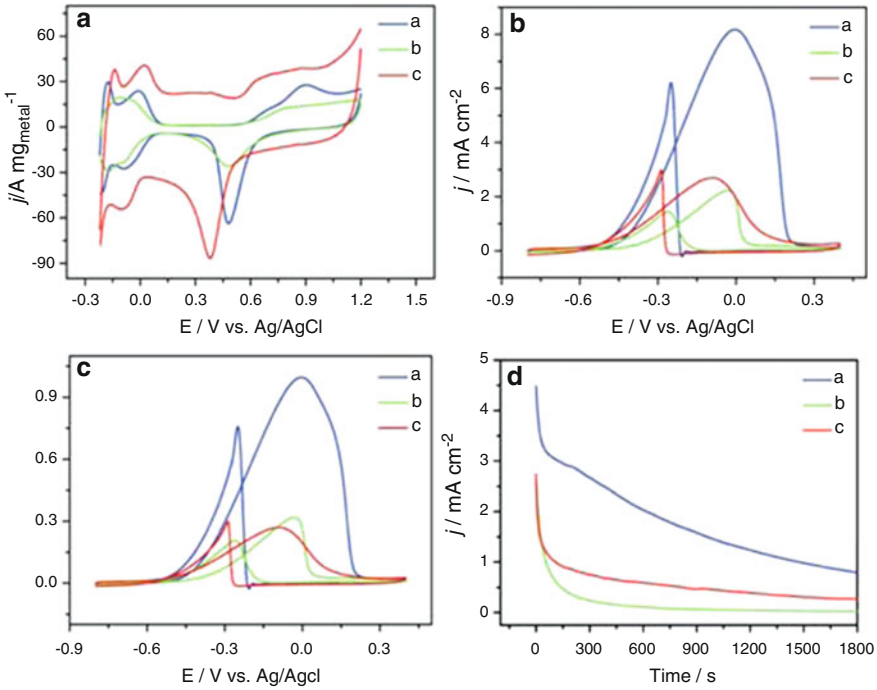

Fig. 4.15 (**a**) CVs of the PBNPSs (curve a), PNPSs (curve b) and E-TEK Pd/C (curve c) electrodes in a 0.5 M H_2SO_4 solution; CVs ((**b**): specific activity; (**c**): mass activity) of the PBNPSs (curve a), PNPSs (curve b) and E-TEK Pd/C (curve c) electrodes in a 0.5 M H_2SO_4+ 1 M ethanol solution at the scan rate of 50 mV/s; (**d**) Current density-time curves (specific activity) of the PBNPSs (curve a), PNPSs (curve b) and E-TEK Pd/C (curve c) electrodes in a 0.5 M NaOH +1 M ethanol solution at −0.2 V. Reprinted with permission from [117]. Copyright 2010 Royal Society of Chemistry

surface area, lower onset potential, and larger current density of ethanol oxidation. This study indicates that PNVC-V_2O_5 polymer-metal composite can serve as a promising catalyst supporting material for fuel cells.

4.3.2 Formic Acid Oxidation Reaction (FAOR)

Formic acid is a liquid at room temperature, and dilute formic acid is recognized as a safe fuel used in low-temperature fuel cells. As compared to traditional hydrogen fuel, aqueous solutions of formic acid exhibit the advantages of ease of transportation, storage and handling. Moreover, direct formic acid fuel cells (DFAFCs) have a smaller crossover of formic acid than that of methanol fuels in DMFCs, which simultaneously improves fuel utilization and enables the use of thinner membranes. In addition, DFAFCs has a theoretical open circuit voltage (OCV) of

about 1.48 or 1.45 V, which is higher than hydrogen-oxygen (1.23 V) and methanol-oxygen (1.18 V) fuel cells [179–181]. For formic acid oxidation, a so-called dual pathway mechanism has been commonly accepted: (i) direct pathway (dehydrogenation pathway), which involves the removal of two hydrogen atoms from formic acid molecule to directly produce CO_2 ($HCOOH \rightarrow CO_2 + 2H^+ + 2e^-$), and (ii) indirect pathway (dehydration pathway), which involves the dehydration of formic acid to yield a poisonous intermediate CO species (CO_{ads}) and then further oxidation to CO_2 ($HCOOH \rightarrow CO_{ads} + H_2O \rightarrow CO_2 + 2H^+ + 2e^-$). On the basis of such a mechanism, to enhance fuel cell efficiency and avoid poisoning, the materials on which the direct dehydrogenation pathway predominantly occurs or have high CO tolerance are ideal anode catalysts for formic acid oxidation. Pt-Pd bimetallic catalysts are considered as a substitute of platinum in fuel cells due to their attractive performance and better CO tolerance during formic acid oxidation than that of Pt catalysts [69, 135, 182].

By controlling the crystallographic orientation of the surface atoms, Pt-Pd bimetallic nanocrystals with enhanced electrochemical properties can be designed [124, 173]. For instance, by using highly faceted cubic Pt as seeds to direct the epitaxial overgrowth of Pd, Yang and coworkers [116] prepared shape-controlled Pt-Pd heterostructures and studied their catalytic activities for formic acid electrooxidation. From the CVs of formic acid oxidation shown in Fig. 4.16, (100)-facets terminated cubic Pt-Pd core-shell particles (Fig. 4.16a) exhibit a much higher peak current that is five times of that from the (111)-facets terminated Pt-Pd octahedra (Fig. 4.16c), whereas the octahedral Pt-Pd shows a lower peak potential (0.15 V) than the cubic Pt-Pd (0.36 V). Moreover, the Pt-Pd cubes show a sharper peak at 0.47 V in the negative scan than the octahedra, and the Pt-Pd cuboctahedra show intermediate catalytic properties between the cubes and octahedra (Fig. 4.16b). The surface-dependent properties can be ascribed to the different arrangement of atoms at the surface of different shaped Pt-Pd nanocrystals, and thus the corresponding surface energy affects adsorption, surface diffusion, intermediate formation, chemical rearrangements and finally desorption of the products in the formic acid oxidation.

In another work, Pt-Pd binary nanoparticles were fabricated by decorating Pd on the well-defined Pt(100) single crystal surface via a seed-mediated growth process [123]. Because the presence of adsorbed Pd on Pt(100) can minimize CO formation at low potential, and thus decrease the self-poisoning and lower the oxidation potential, the prepared Pt-Pd nanoparticles showed remarkably enhanced electrocatalytic performance for formic acid oxidation. Feliu and coworkers [145] prepared Pd adatom-modified (100) preferentially oriented cubic Pt nanoparticles by an electrochemical deposition approach using a reductant- and surfactant-free process. In electrochemical measurements, the formic acid oxidation current was strongly inhibited in the positive scan on the bare cubic Pt nanoparticles owing to the almost complete poisoning of (100) surface sites by CO. After the incorporation of Pd, the formic acid oxidation was enhanced. However, due to the lower fraction of Pt(100) sites in the quasispherical Pt nanoparticles, the current density obtained from the cubic Pt nanoparticles is higher than that from quasispherical Pt

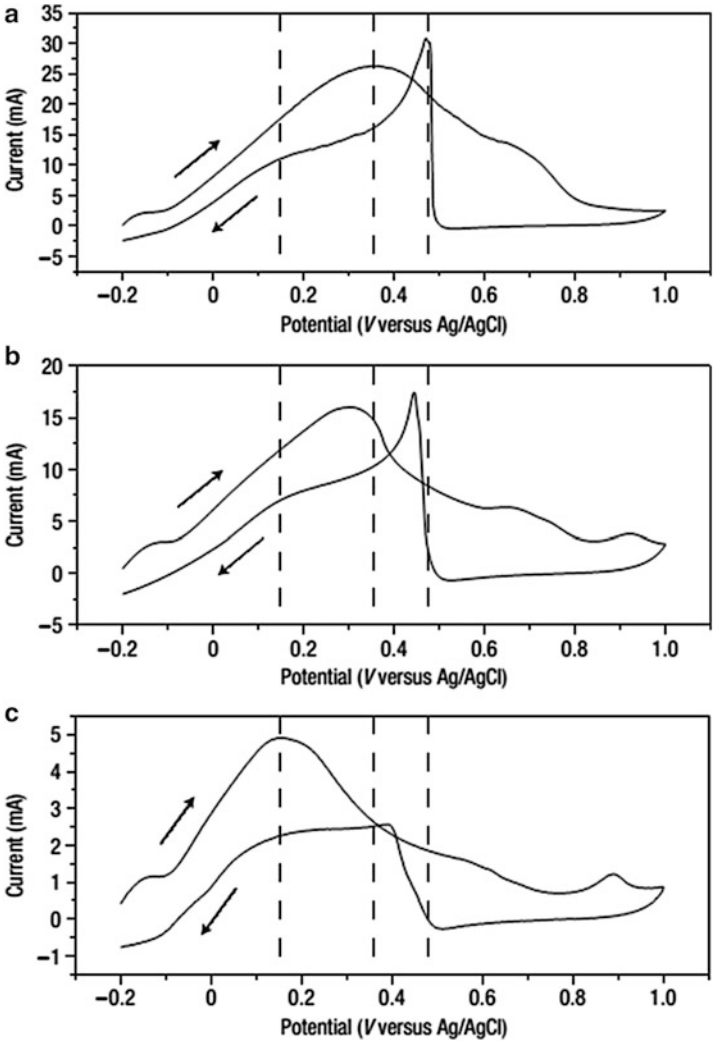

Fig. 4.16 Electrocatalytic activities of the Pt-Pd binary metal nanocrystals for formic acid oxidation. (**a**–**c**) Cyclic voltammograms for cubes (**a**), cuboctahedra (**b**) and octahedra (**c**) in 0.1 M H_2SO_4 and 0.2 M formic acid at a sweep rate of 50 mV/s. Reprinted with permission from [116]. Copyright 2007 Nature Publishing Group

nanoparticles. Moreover, the Pd adatom-decorated cubic Pt nanoparticles exhibited high stability during the formic acid oxidation. Such results indicate that modification of shape-controlled Pt by surface adatoms is an efficient strategy to enhance their electrocatalytic activities.

It was also found that the catalytic activities of Pt-Pd bimetallic nanocrystals towards formic acid electro-oxidation depend on their compositions [67, 183]. Zheng and coworkers [111] reported that Pt can be alloyed into the Pd

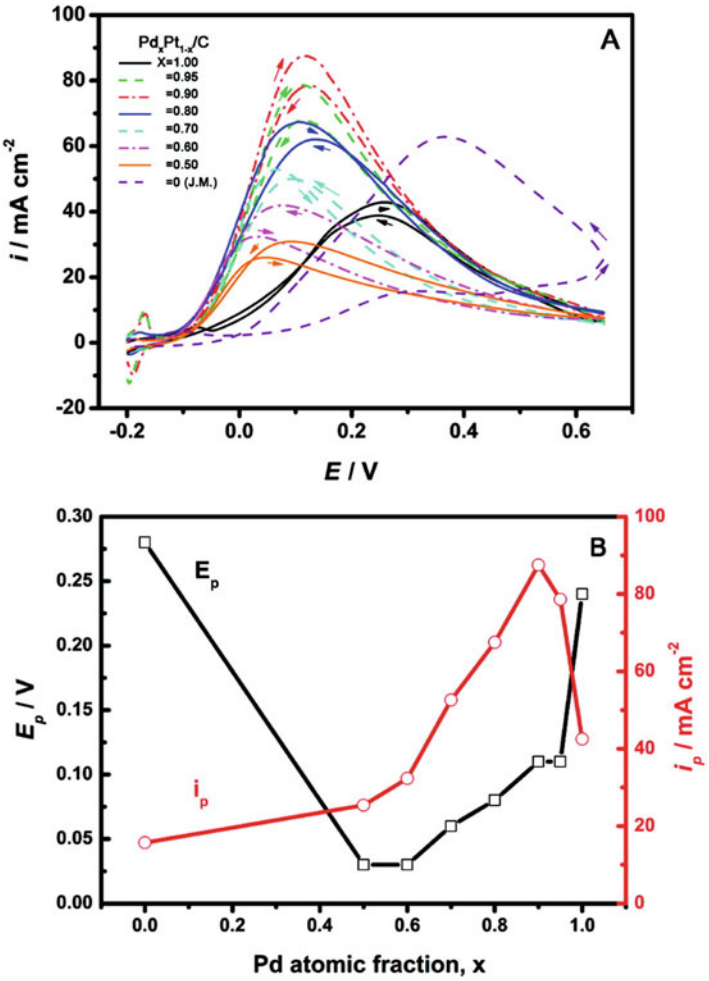

Fig. 4.17 (**a**) Cyclic voltammograms recorded at 50 mV/s for Pd_xPt_{1-x}/C coated on GC electrodes in 0.5 M H_2SO_4 solution containing 0.5 M formic acid. (**b**) Variation of E_p and i_p with Pd atomic fraction (x). Reprinted with permission from [51]. Copyright 2010 American Chemical Society

nanospheres and the Pt-Pd nanoparticles with a molar ratio of Pd/Pt = 3:1 exhibited the highest activity for electrocatalytic oxidation of formic acid. Cai and coworkers [51] synthesized a series of Pd_xPt_{1-x} ($x = 0.5$–1) nanoparticles dispersed on carbon black support and studied their catalytic activities for formic acid oxidation. Figure 4.17a compares the CVs of formic acid oxidation on different compositions of Pd_xPt_{1-x}/C catalysts in 0.5 M H_2SO_4 solution containing 0.5 M formic acid (FA). Obviously, the peak current density (i_p) of FA oxidation is x-dependent, and the $Pd_{0.9}Pt_{0.1}$/C shows the highest i_p which is nearly twice as high as that of Pd/C and

six times of that of commercial Pt/C. The larger gap of negatively shifted peak potentials (Fig. 4.17b) between Pd/C and $Pd_{0.9}Pt_{0.1}$/C but smaller difference between Pd_xPt_{1-x}/C catalysts demonstrate the synergistic effect of Pd and Pt sites in the FA electro-oxidation. Moreover, after 1000 s stability test, the oxidation current density on $Pd_{0.9}Pt_{0.1}$/C is the highest among the Pd_xPt_{1-x}/C catalysts, which is 2.4- and 3.6-fold larger than those of commercial Pd/C and Pt/C, respectively.

Carbon nanotubes have also exhibited their potential applications as catalyst supports in fuel cells [71]. Chen and coworkers [99] studied the catalytic properties of hollow Pt-Pd nanospheres dispersed on carbon nanotubes. The electrochemical measurements showed that the prepared hybrids have enhanced activity with a high peak current and steady-state current toward formic acid oxidation as compared to commercial Pt/C and E-TEK PtRu/C. In another study, Pt_xPd_y alloy nanoparticles supported on carbon nanotubes were also studied as anode catalysts for FAOR [59]. It was found that the catalytic activity and stability of the CNT-supported catalysts increase with more Pd content in the catalysts. In addition, titanium [92] and conductive polymer (polythiophene) [138] were also employed as support materials to disperse Pt-Pd bimetallic nanocrystal with enhanced electrocatalytic activities for formic acid oxidation.

4.3.3 Oxygen Reduction Reaction (ORR)

Oxygen reduction reaction (ORR) on cathode plays a crucial role in manipulating the performance of a fuel cell. Whereas much progress has been achieved on cathodic catalysts in the past few decades, the inherently slow reaction kinetics of ORR and the large overpotential still prevent the fuel cells from being scaled-up for commercial applications. The ORR has complicated reaction pathways and involves a multi-electron transfer process in which O_2 is converted into H_2O or OH^-, depending on the solution used in the electrochemical studies. In an acidic solution, O_2 can be reduced in an efficient $4e^-$ process and converted into H_2O: $O_2 + 4e^- \rightarrow 2H_2O$. Meanwhile, O_2 may also undergo a less efficiently partial $2e^-$ reduction to form hydrogen peroxide, H_2O_2, followed by another $2e^-$ reduction to convert H_2O_2 into H_2O: $O_2 + 2H^+ + 2e^- \rightarrow H_2O_2$; $H_2O_2 + 2H^+ + 2e^- \rightarrow 2H_2O$. In alkaline solution, O_2 can be reduced by a $4e^-$ process to form hydroxide, OH^-: $O_2 + 2H_2O + 4e^- \rightarrow 4OH^-$, or by two $2e^-$ processes to form HO_2^- and then OH^-: $O_2 + H_2O + 2e^- \rightarrow HO_2^- + OH^-$; $HO_2^- + H_2O + 2e^- \rightarrow 3OH^-$. In addition, under common ORR conditions, oxygen may be converted into different intermediates, such as oxygenated (O), hydroxyl (OH) and superhydroxyl (OOH) species, which are very difficult to be detected experimentally [184].

The kinetic parameters of ORR can be determined using the rotating disk electrode (RDE) technique. The kinetic current density and the electron transfer numbers can be derived from the following equations: [14]

$$\frac{1}{j} = \frac{1}{j_K} + \frac{1}{j_L} = \frac{1}{j_K} + \frac{1}{B^{1/2}} \tag{4.1}$$

$$B = 0.2nF(D_0)^{2/3}\nu^{-1/6}C_0 \tag{4.2}$$

$$j_K = nFkC_0 \tag{4.3}$$

where j is the measured current density, j_K and j_L are the kinetic and diffusion limitation current densities, ω is the electrode rotating rate, n represents the number of electrons transferred per oxygen molecule, F is the Faraday constant (F= 96,485 C/mol), D_0 is the diffusion coefficient of O_2, ν is the kinetic viscosity of the electrolyte, and C_0 is the bulk concentration of O_2 dissolved in the electrolyte. The constant 0.2 is used when the rotation speed is expressed in rpm. According to Eqs. 4.1–4.3, the number of electron transfer (n) and kinetic current density (j_K) can be obtained from the slope and intercept of the Koutecky-Levich plots, respectively. In addition, rotating ring-disk electrode (RRDE) can also be used to evaluate the ORR performance of a catalyst. Electron transfer number (n) and the H_2O_2 percentage (H_2O_2%) generated at the disk electrode can be calculated from the ring and disk current as the following equations (i_D and i_R represent the disk and ring current, and N is the RRDE collection efficiency) [185]:

$$n = \frac{4i_D}{i_D + i_R/N} \tag{4.4}$$

$$H_2O_2\% = \frac{200i_R/N}{i_D + i_R/N} \tag{4.5}$$

At present, because of the outstanding catalytic properties, Pt has been the most widely used electrocatalyst to speed up oxygen reduction at cathode. However, despite extensive research efforts, the sluggish oxygen reduction kinetics at the cathode, high cost, low stability and limited supply of platinum still largely restrict the wide spread commercialization of fuel cells. Moreover, the state-of-art commercial catalysts are usually prepared by dispersing Pt nanoparticles (2–5 nm) on carbon supports, whose electrochemical surface areas and catalytic efficiency degrade over time owing to the corrosion of the carbon supports and the dissolution, aggregation of Pt nanoparticles during the catalysis processes. This has posed tremendous challenges in the development of Pt-based catalysts for practical fuel-cell applications. The combination of Pd with Pt can downshift the d-band center of Pt catalyst, leading to a lower degree of adsorption of oxygenated spectator species (such as OH^-) and an increase of the number of active sites accessible to oxygen, Pt-Pd bimetallic nanocrystals have been accepted as one type of the most active and effective cathodic catalysts for oxygen reduction reaction.

The enhancement of the Pt mass or specific activity for ORR can be achieved by controlling the composition of the alloyed Pt-Pd nanomaterials [38–40, 56, 60, 73]. Cooks and coworkers [35] prepared Pt-Pd bimetallic nanoparticles (~1.8 nm) containing an average of 180 atoms with seven different Pt:Pd ratios

(G6-OHPt_nPd_{180-n}DENs, n = 180, 150, 120, 90, 60, 30 and 0) by a dendrimer templating method. From the results of CV and rotating disk voltammetry measurements shown in Fig. 4.18, as compared to the equivalent monometallic Pt DENs catalyst, the maximum relative mass activity enhancement of 240% was obtained from the bimetallic PtPd DENs containing 17–33% Pd. And the G6-OH ($Pt_{150}Pd_{30}$) DENs exhibited the most active ORR performance with the most positive onset potential, the highest kinetic current density and an efficient $4e^-$ oxygen reduction process. Huang and coworkers studied the ORR activity of the Pt-Pd bimetallic nanocrystals with different compositions [115]. It was found that the bimetallic Pt-Pd nanocrystals have higher ORR activity than that of commercially available Pt black and Pd black in acid solution, and the bimetallic nanocrystals with Pd/Pt ratio of 1/3 gave the highest ORR activity. Lee et al. [70] reported that the Pt-Pd nanocatalysts deposited on Vulcan XC-72R carbon support with a molar ratio of 1:3 exhibited much enhanced catalytic activity toward oxygen reduction reaction in comparison with commercial Pt/C. By using carbon nanotubes as supports for electrocatalyst, Ghosh et al. [55] investigated the catalytic properties of multiwalled

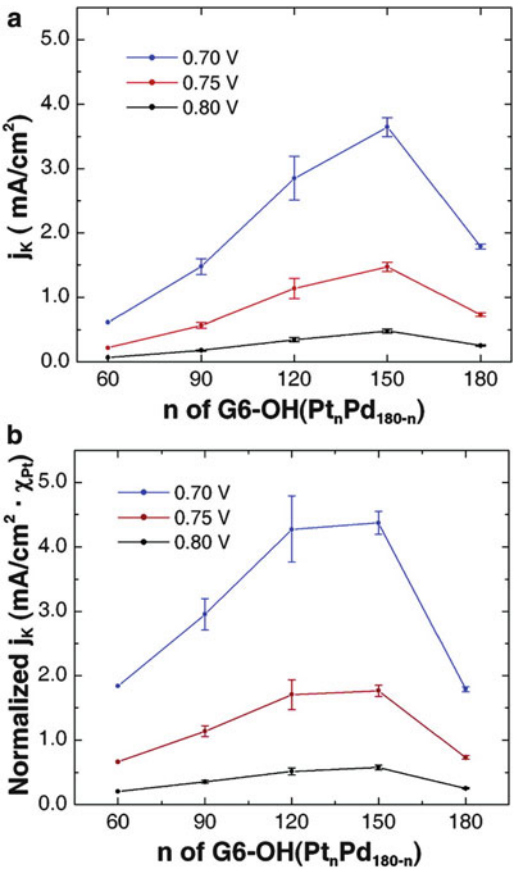

Fig. 4.18 Plots of (**a**) kinetic current density and (**b**) kinetic current density normalized to the fraction amount of Pt contained in each nanoparticle composition at different potentials. Error bars represent the span of data for two independently executed experiments (only one experiment was carried out for G6-OH ($Pt_{60}Pd_{120}$). Reprinted with permission from [35]. Copyright 2007 American Chemical Society

carbon nanotubes (MCNTs)-supported Pt-Pd nanoparticles with different compositions. The electrochemical measurements showed that the $Pt_{46}Pd_{54}$ nanoparticles supported on MCNTs have an enhanced electrocatalytic activity toward ORR with specific and mass activities of 378 $\mu A/cm^2_{Pt\text{-}Pd}$ and 64 $\mu A/\mu g_{Pt\text{-}Pd}$ at 0.8 V, as compared to 150 $\mu A/cm^2_{Pt\text{-}Pd}$ and 26.5 $\mu A/\mu g_{Pt\text{-}Pd}$ for $Pt_{64}Pd_{36}$, 33 $\mu A/cm^2_{Pt\text{-}Pd}$ and 4.5 $\mu A/\mu g_{Pt\text{-}Pd}$ for $Pt_{28}Pd_{72}$, and 142 $\mu A/cm^2_{Pt\text{-}Pd}$ and 45.7 $\mu A/\mu g_{Pt\text{-}Pd}$ for commercial Pt black. Moreover, the $Pt_{46}Pd_{54}$/MCNTs exhibited high stability and tolerance to methanol during the oxygen reduction. The synergistic effect between Pt and Pd and the strong MCNT-catalyst interaction was believed to enhance the overall catalytic performance of the catalysts.

In addition to composition, the catalytic activities of Pt-Pd bimetallic nanocrystals toward ORR are also dependent on their shapes. Pt-Pd core-shell nanocrystals are a class of electrocatalysts for ORR with an enhanced performance. For example, Iwasawa and coworkers [114] investigated the catalytic activities of three types of bimetallic Pt-Pd nanoparticles, Pt/C, Pd (core)-Pt (shell), and Pt (core)-Pd (shell) for ORR. By comparing the CVs, the Pt/C, PdPt alloy/C, and Pd (core)-Pt (shell)/C catalysts with Pt-enriched surfaces showed much higher ORR specific activities than the Pd/C and Pt (core)-Pd (shell)/C catalysts with Pd-enriched surfaces. And the Pt surface-enriched bimetallic catalysts with a core-shell structure showed higher Pt-based mass activity than the Pt monometal catalyst. Moreover, after 1000 cycles of CV test, the loss of ECSA is less than 20% for Pd (core)-Pt (shell)/C and PdPt alloy/C with Pt-enriched surfaces, while drop as large as 53.8% and 41.6% for Pd/C and Pt (core)-Pd (shell)/C with Pd-enriched surfaces, suggesting that Pt surface-enriched catalysts have great stability in ORR.

Pt monolayer deposited on Pd provides another promising core-shell structure to enhance the ORR activity through the strong interaction between these two metals, as well as the reduction of Pt loading down to a minimum level [110, 146, 148, 150, 186, 187]. Adzic and coworkers [153] reported a synthesis of well-defined Pd core-Pt monolayer shell nanocatalysts for ORR. It was found that the optimized Pt monolayer on commercial Pd nanoparticles exhibited outstanding mass and area-specific ORR activities of 0.96 A/mg_{Pt} and 0.5 mA/cm^2, respectively. The significant enhancement in activity could be attributed to the uniquely advantageous core-shell motif. In the structure, the Pd core imparts a compressive strain and a so-called "ligand-effect" upon the Pt monolayer, which can effectively lower the energy of the Pt d-band and thus directly weaken its interaction with OH_{ads} group, thereby yielding improved ORR activity. Sasaki et al. [151] investigated the catalytic performance of a Pd core-protected Pt monolayer shell catalyst for ORR. Compared to commercial Pt/Ketjen black and Pt/C, the Pd nanoparticles covered by a Pt monolayer (Pt ML/Pd/C) exhibited much higher electrocatalytic durability. The mass activity of the Pt ML/Pd/C decreased by 37% after 100,000 cycles of stability tests, while the mass activity of Pt/C lost almost 70% after 60,000 potential cycles and the Pt/Ketjen black carbon experienced more than 40% loss after only 10,000 cycles. Surprisingly, due to the effect of potential cycling on the particle size distribution, the Pt mass activity of PtML/Pd/C

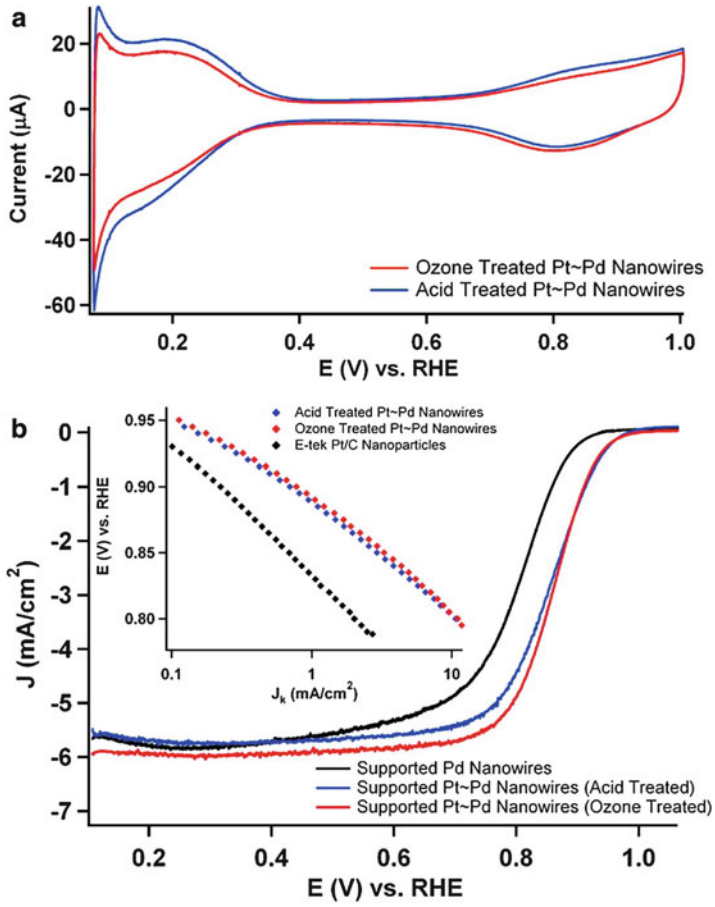

Fig. 4.19 Cyclic voltammograms (**a**) obtained for the ozone- and acid-treated Pt-PdNW/C core-shell nanowires, after Pt monolayer deposition, loaded separately onto a GCE in a 0.1 M $HClO_4$ solution at 20 mV/s. (**b**) The polarization curves for the treated Pt-Pd/C core-shell nanowire composites were both obtained on a glassy carbon rotating disk electrode. Curves (anodic sweep direction) were collected using a rotation rate of 1600 rpm in a 0.1 M $HClO_4$ solution at 20 ˚C. Kinetic current vs potential plots (inset) of treated Pt-Pd/C composites and commercial carbon supported Pt nanoparticles are also presented. Reprinted with permission from [152]. Copyright 2011 American Chemical society

increased from the initial 3-fold to 5-fold enhancement over that of Pt/C after 60,000 cycles.

In another work, Adzic and coworkers [152] reported the deposition of a monolayer quantity of Pt onto the surface of the treated Pd nanowires/C (Pd NW/C) composites by Cu UPD followed by galvanic replacement of the Cu adatoms with Pt^{2+}, and their electrocatalytic activity for ORR in acid condition. As shown in Fig. 4.19a, b, the ultrathin Pt monolayer shell-Pd nanowire core catalyst (Pt-Pd NW/C) displayed dramatically enhanced ORR activity compared to the Pd

NW/C and commercial Pt nanoparticles. Moreover, the ozone-treated Pt-Pd NW/C exhibited much higher area-specific (0.77 mA/cm^2) and mass-specific (1.83 A/mg_{Pt}) activities than those of acid-treated Pt-Pd nanowires (0.70 mA/cm^2 and 1.47 A/mg_{Pt}). Such results indicate that the ozone treatment for Pd NW before Cu UPD can lead to the exceptional enhancement in the catalytic activity of Pt-Pd nanowires. Most importantly, after the accelerated durability half-cell test, the ozone-treated Pt-Pd nanowires still maintained excellent electrochemical durability and the area-specific activity increased by 1.5-fold.

Pt-Pd nanodendrites are another novel structure imparting its enhanced ORR activity by maximizing the expression of certain highly active facets and improving surface area. Xia and coworkers [122] synthesized Pt-Pd bimetallic nanodendrites consisting of a dense array of Pt branches on a Pd core, and investigated their catalytic activity for ORR in acid conditions. The calculated ECSA of the Pt-Pd nanodendrites (57.1 m^2/g_{Pt}) is much larger than that of commercial Pt black catalyst (19.1 m^2/g_{Pt}), but is lower than that of Pt/C catalyst (74 m^2/g_{Pt}). It was found that the mass activity from the Pt-Pd nanodendrites (0.241 $mA/\mu g_{Pt}$) is 2.5- and 5-fold larger, respectively, than those of state-of-art Pt/C and the first-generation supportless Pt-black catalyst at room temperature. Moreover, at 60 °C, the Pt mass activity of the Pt-Pd nanodendrites (0.433 $mA/\mu g_{Pt}$) was still greater than that of the Pt/C catalyst (0.204 $mA/\mu g_{Pt}$) and the Pt black (0.078 $mA/\mu g_{Pt}$). In addition to mass activity, Pt-Pd nanodendrites exhibited a specific activity of 3.1–3.4-fold that of the Pt/C catalyst and 1.7–2.0-fold that of the Pt black depending on the temperature, indicating a superior capability of the Pt-Pd nanodendrites in accelerating ORR. The high ORR activity of the Pt-Pd nanodendrites can be attributed to the high and accessible surface area of the dendritic morphology and the preferential exposure of (1 1 1) facets along with some (1 1 0) and high-index (3 1 1) facets on the Pt branches that are particularly active towards ORR. In another work, Yang and coworkers [126] reported the synthesis of Pt-on-Pd heteronanostructure supported on carbon black. The as-synthesized nanostructure showed much larger electrochemically active surface area as compared to E-TEK Pt/C (20 wt%Pt) catalyst (Fig. 4.20a). From Fig. 4.20b, it can be seen that the incorporation of Pd also greatly altered the ability to absorb hydroxyl species (OH_{ads}, $E > 0.6$ V) compared to E-TEK Pt/C (20 wt%Pt) catalyst, and the Pt-on-Pd catalyst exhibited much faster hydroxyl desorption ability with positively shifted onset and peak potentials in the backward sweep. As shown in Fig. 4.20c, d, the Pt-on-Pd catalyst shows a more positive onset potential and higher activity than the commercially pure Pt. Moreover, after 30,000 cyclic voltammetry cycling, the Pt-on-Pd catalyst lost only 12% of the initial ECSA and showed a small degradation of 9 mV in the half-wave potential, while a loss of 39% of the initial ECSA and a large decrease of 35 mV in the half-wave potential for Pt/C catalyst, suggesting the enhanced stability of Pt-on-Pd/C catalyst for ORR.

In addition, the ORR catalytic activities of Pt-Pd bimetallic nanostructures with other specific size and morphologies such as hollow urchin-like [97], bowl-like [100], and rods [77], were also investigated. Yan et al. [101] found that Pt-Pd nanotubes exhibited much enhanced ORR mass/specific activity, and improved

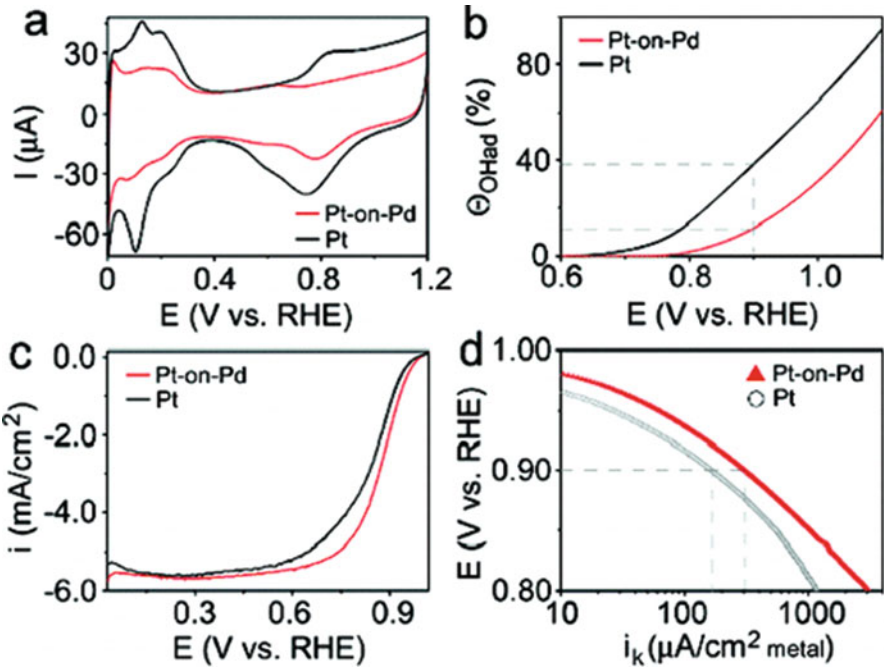

Fig. 4.20 (**a**) CVs, (**b**) hydroxyl surface coverage (Θ_{OH}), (**c**) ORR polarization curves, and (**d**) specific kinetic current densities (i_k) for carbon-supported Pt-on-Pd and Pt catalysts. Reprinted with permission from [126]. Copyright 2009 American Chemical Society

stability in acid electrolyte as compared to commercial Pt/C and Pt black catalysts. As reported by Xia and coworkers in another work [102], Pt-Pd concave cubes with different weight percentages of Pt can be prepared by using bromide-induced galvanic replacement method. It was found that the ORR activities of the Pt-Pd concave nanocubes on the basis of Pt mass monotonically increase with decreasing Pt weight percentage. And the Pt-Pd concave nanocubes with a Pt weight percentage of 3.4 showed the highest mass activity for ORR, which is 4 times higher than that of the Pt/C catalyst in terms of equivalent Pt mass. In a recent work from our group [104], Pt-Pd porous nanorods (PtPd PNRs) were successfully synthesized through a bromide-induced galvanic replacement reaction between Pd nanowires (Pd NWs) and K_2PtCl_6. The unique porous Pt-Pd nanorods showed greatly enhanced ORR activity with the highest limiting current densities and the most positive onset potential compared to those obtained from the original Pd NWs and commercial Pt/C catalyst. In addition to the improved catalytic activity, the PtPd PNRs also showed excellent durability in ORR (Fig. 4.21a–d) with only 5.88% loss of the initial ECSA after the accelerated durability tests (1000 potential cycles), whereas 21.6% and 40.4% of their original ECSA were lost for the Pd NWs and commercial Pt/C catalyst, respectively. The enhanced catalytic activity of PtPd

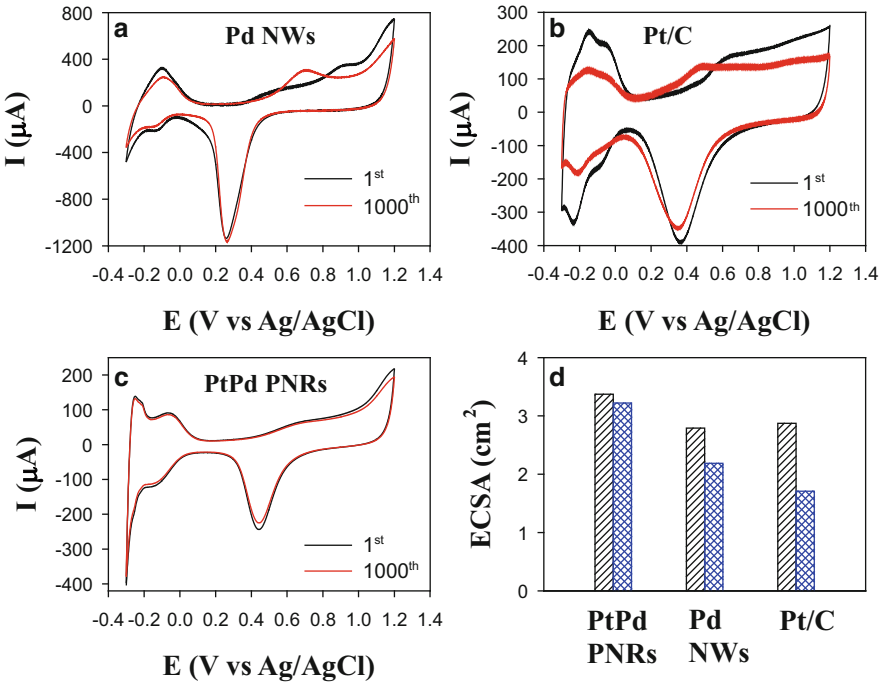

Fig. 4.21 Cyclic voltammograms recorded on Pd NWs (**a**), Pt/C (**b**) and PtPd PNRs (**c**) before (*black curves*) and after 1000 cycles (*red curves*) of the accelerated durability test, in 0.1 M $HClO_4$ solution with a potential scan rate of 0.1 V/s. (**d**) Comparison of the electrochemical surface area (ECSA) before and after 1000 cycles of the accelerated durability tests on the PtPd PNRs, Pd NWs, and commercial Pt/C catalyst, respectively. Reprinted with permission from [104]. Copyright 2013 Elsevier

PNRs toward ORR with efficient $4e^-$ pathway can be ascribed to its high specific surface area, unique one-dimensional morphology and the alloy structure.

4.4 Conclusion

Over the past several years, Pt-Pd bimetallic nanocrystals have received great attention owing to their attractive properties and extensive applications in fuel cells. In this chapter, the recent development related to the synthesis of Pt-Pd bimetallic nanocrystals with different structures, including Pt-Pd alloys, core-shell, multi-shells, dendrites and supported monolayer has been extensively reviewed. Furthermore, a number of strategies based on co-chemical reduction, galvanic displacement, seed-mediated growth and the combination of these methods used to control the formation of Pt-Pd bimetallic nanocrystals with a specific structure have been discussed. Finally, the application of Pt-Pd

(or supported Pt-Pd) bimetallic nanocrystals in fuel cells as catalysts for fuels oxidation at anode and oxygen reduction reaction at cathode was summarized.

Despite substantial progress that has been made in designing Pt-Pd bimetallic electrocatalysts and understanding their electrocatalytic mechanism, the development of new methodologies, the rational control on size, shape, structure and composition of bimetallic nanocrystals, in-depth understanding of the structure-catalytic property relationship, and the exploration of more extensive applications of bimetallic nanocrystals in fuel cells still need to be continuously studied.

Acknowledgements This work was supported by the National Natural Science Foundation of China with the Grant Numbers of 21275136, 21043013 and the Natural Science Foundation of Jilin Province, China (No. 201215090).

References

1. Potocnik J (2007) Renewable energy sources and the realities of setting an energy agenda. Science 315:810–811
2. Armand M, Tarascon JM (2008) Building better batteries. Nature 451:652–657
3. Steele BCH, Heinzel A (2001) Materials for fuel-cell technologies. Nature 414:345–352
4. Russell AE, Rose A (2004) X-ray absorption spectroscopy of low temperature fuel cell catalysts. Chem Rev 104:4613–4635
5. Lamy C, Lima A, LeRhun V, Delime F, Coutanceau C, Leger JM (2002) Recent advances in the development of direct alcohol fuel cells (DAFC). J Power Sources 105:283–296
6. Vigier F, Rousseau S, Coutanceau C, Leger JM, Lamy C (2006) Electrocatalysis for the direct alcohol fuel cell. Top Catal 40:111–121
7. Tian N, Zhou ZY, Sun SG, Ding Y, Wang ZL (2007) Synthesis of tetrahexahedral platinum nanocrystals with high-index facets and high electro-oxidation activity. Science 316:732–735
8. Chen W, Kim J, Sun SH, Chen SW (2006) Electro-oxidation of formic acid catalyzed by FePt nanoparticles. Phys Chem Chem Phys 8:2779–2786
9. Chen W, Kim JM, Sun SH, Chen SW (2007) Composition effects of FePt alloy nanoparticles on the electro-oxidation of formic acid. Langmuir 23:11303–11310
10. Yang HZ, Zhang J, Sun K, Zou SZ, Fang JY (2010) Enhancing by weakening: electrooxidation of methanol on Pt_3Co and Pt nanocubes. Angew Chem Int Ed 49:6848–6851
11. Chen YX, Miki A, Ye S, Sakai H, Osawa M (2003) Formate, an active intermediate for direct oxidation of methanol on Pt electrode. J Am Chem Soc 125:3680–3681
12. Tripkovic AV, Popovic KD, Grgur BN, Blizanac B, Ross PN, Markovic NM (2002) Methanol electrooxidation on supported Pt and PtRu catalysts in acid and alkaline solutions. Electrochim Acta 47:3707–3714
13. Qiao Y, Li CM (2011) Nanostructured catalysts in fuel cells. J Mater Chem 21:4027–4036
14. Zhang RZ, Chen W (2013) Non-precious Ir-V bimetallic nanoclusters assembled on reduced graphene nanosheets as catalysts for the oxygen reduction reaction. J Mater Chem A 1:11457–11464
15. Liu MM, Zhang RZ, Chen W (2014) Graphene-supported nanoelectrocatalysts for fuel cells: synthesis, properties, and applications. Chem Rev 114:5117–5160
16. Zhang H, Jin MS, Xia YN (2012) Enhancing the catalytic and electrocatalytic properties of Pt-based catalysts by forming bimetallic nanocrystals with Pd. Chem Soc Rev 41:8035–8049
17. Gasteiger HA, Markovic N, Ross PN, Cairns EJ (1994) Temperature-dependent methanol electrooxidation on well-characterized Pt-Ru alloys. J Electrochem Soc 141:1795–1803

18. Dinh HN, Ren XM, Garzon FH, Zelenay P, Gottesfeld S (2000) Electrocatalysis in direct methanol fuel cells: in-situ probing of PtRu anode catalyst surfaces. J Electroanal Chem 491:222–233
19. Wang DS, Li YD (2011) Bimetallic nanocrystals: liquid-phase synthesis and catalytic applications. Adv Mater 23:1044–1060
20. Calvo SR, Balbuena PB (2007) Theoretical analysis of reactivity on Pt(111) and Pt-Pd(111) alloys. Surf Sci 601:4786–4792
21. Calvo SR, Balbuena PB (2007) Density functional theory analysis of reactivity of Pt_xPd_y alloy clusters. Surf Sci 601:165–171
22. Norskov JK, Bligaard T, Rossmeisl J, Christensen CH (2009) Towards the computational design of solid catalysts. Nat Chem 1:37–46
23. Norskov JK, Abild-Pedersen F (2009) Catalysis bond control in surface reactions. Nature 461:1223–1225
24. Kitchin JR, Norskov JK, Barteau MA, Chen JG (2004) Role of strain and ligand effects in the modification of the electronic and chemical properties of bimetallic surfaces. Phys Rev Lett 93:156801–156804
25. Hammer B, Norskov JK (2000) Theoretical surface science and catalysis-calculations and concepts. Adv Catal 45:71–129
26. Norskov JK, Rossmeisl J, Logadottir A, Lindqvist L, Kitchin JR, Bligaard T, Jonsson H (2004) Origin of the overpotential for oxygen reduction at a fuel-cell cathode. J Phys Chem B 108:17886–17892
27. de Bruijn FA, Dam VAT, Janssen GJM (2008) Durability and degradation issues of PEM fuel cell components. Fuel Cells 8:3–22
28. Stamenkovic VR, Fowler B, Mun BS, Wang GF, Ross PN, Lucas CA, Markovic NM (2007) Improved oxygen reduction activity on $Pt_3Ni(111)$ via increased surface site availability. Science 315:493–497
29. Ramirez-Caballero GE, Hirunsit P, Balbuena PB (2010) Shell-anchor-core structures for enhanced stability and catalytic oxygen reduction activity. J Chem Phys 133:134705–134713
30. Xia YN, Xiong YJ, Lim B, Skrabalak SE (2009) Shape-controlled synthesis of metal nanocrystals: simple chemistry meets complex physics? Angew Chem Int Ed 48:60–103
31. Shao YY, Yin GP, Gao YZ (2007) Understanding and approaches for the durability issues of Pt-based catalysts for PEM fuel cell. J Power Sources 171:558–566
32. Ferreira PJ, La O' GJ, Shao-Horn Y, Morgan D, Makharia R, Kocha S, Gasteiger HA (2005) Instability of Pt/C electrocatalysts in proton exchange membrane fuel cells—a mechanistic investigation. J Electrochem Soc 152:A2256–A2271
33. Wang YJ, Wilkinson DP, Zhang JJ (2011) Noncarbon support materials for polymer electrolyte membrane fuel cell electrocatalysts. Chem Rev 111:7625–7651
34. Greeley J, Stephens IEL, Bondarenko AS, Johansson TP, Hansen HA, Jaramillo TF, Rossmeisl J, Chorkendorff I, Norskov JK (2009) Alloys of platinum and early transition metals as oxygen reduction electrocatalysts. Nat Chem 1:552–556
35. Ye HC, Crooks RM (2007) Effect of elemental composition of PtPd bimetallic nanoparticles containing an average of 180 atoms on the kinetics of the electrochemical oxygen reduction reaction. J Am Chem Soc 129:3627–3633
36. Yang SC, Hong F, Wang LQ, Guo SW, Song XP, Ding BJ, Yang ZM (2010) Ultrathin Pt-based alloy nanowire networks: synthesized by CTAB assistant two-phase water-chloroform micelles. J Phys Chem C 114:203–207
37. Basu D, Basu S (2012) Performance studies of Pd-Pt and Pt-Pd-Au catalyst for electrooxidation of glucose in direct glucose fuel cell. Int J Hydrogen Energy 37:4678–4684
38. Thanasilp S, Hunsom M (2011) Preparation of a high-performance Pt-Pd/C-electrocatalyst-coated membrane for ORR in PEM fuel cells via a combined process of impregnation and seeding: effect of electrocatalyst loading on carbon support. Electrochim Acta 56:1164–1171

39. Thanasilp S, Hunsom M (2011) Effect of Pt: Pd atomic ratio in Pt-Pd/C electrocatalyst-coated membrane on the electrocatalytic activity of ORR in PEM fuel cells. Renew Energy 36:1795–1801
40. Tang YF, Zhang HM, Zhong HX, Xu T, Jin H (2011) Carbon-supported Pd-Pt cathode electrocatalysts for proton exchange membrane fuel cells. J Power Sources 196:3523–3529
41. Maghsodi A, Hoseini MRM, Mobarakeh MD, Kheirmand M, Samiee L, Shoghi F, Kameli M (2011) Exploration of bimetallic Pt-Pd/C nanoparticles as an electrocatalyst for oxygen reduction reaction. Appl Surf Sci 257:6353–6357
42. Li XW, Zhu Y, Zou ZQ, Zhao MY, Li ZL, Zhou Q, Akins DL, Yang H (2009) Simple complexing-reduction synthesis of Pd-Pt/C alloy electrocatalysts for the oxygen reduction reaction. J Electrochem Soc 156:B1107–B1111
43. Kim IT, Lee HK, Shim J (2008) Synthesis and characterization of Pt-Pd catalysts for methanol oxidation and oxygen reduction. J Nanosci Nanotechnol 8:5302–5305
44. Joo JB, Kim YJ, Kim W, Kim ND, Kim P, Kim Y, Yi J (2008) Methanol-tolerant PdPt/C alloy catalyst for oxygen electro-reduction reaction. Korean J Chem Eng 25:770–774
45. Golikand AN, Asgari M, Lohrasbi E (2011) Study of oxygen reduction reaction kinetics on multi-walled carbon nano-tubes supported Pt-Pd catalysts under various conditions. Int J Hydrogen Energy 36:13317–13324
46. Golikand AN, Lohrasbi E, Asgari M (2010) Enhancing the durability of multi-walled carbon nanotube supported by Pt and Pt-Pd nanoparticles in gas diffusion electrodes. Int J Hydrogen Energy 35:9233–9240
47. Morales-Acosta D, Arriaga LG, Alvarez-Contreras L, Luna SF, Varela FJR (2009) Evaluation of $Pt_{40}Pd_{60}$/MWCNT electrocatalyst as ethylene glycol-tolerant oxygen reduction cathodes. Electrochem Commun 11:1414–1417
48. Golikand AN, Lohrasbi E, Maragheh MG, Asgari M (2009) Carbon nano-tube supported Pt-Pd as methanol-resistant oxygen reduction electrocatalyts for enhancing catalytic activity in DMFCs. J Appl Electrochem 39:2421–2431
49. Datta J, Dutta A, Biswas M (2012) Enhancement of functional properties of PtPd nano catalyst in metal-polymer composite matrix: application in direct ethanol fuel cell. Electrochem Commun 20:56–59
50. Wu M, Shen PK, Wei ZD, Song SQ, Nie M (2007) High activity PtPd-WC/C electrocatalyst for hydrogen evolution reaction. J Power Sources 166:310–316
51. Zhang HX, Wang C, Wang JY, Zhai JJ, Cai WB (2010) Carbon-Supported Pd-Pt nanoalloy with low Pt content and superior catalysis for formic acid electro-oxidation. J Phys Chem C 114:6446–6451
52. Godinez-Garcia A, Gervasio DF (2014) Pd-Pt nanostructures on carbon nanofibers as an oxygen reduction electrocatalyst. RSC Adv 4:42009–42013
53. Tao F, Grass ME, Zhang YW, Butcher DR, Renzas JR, Liu Z, Chung JY, Mun BS, Salmeron M, Somorjai GA (2008) Reaction-driven restructuring of Rh-Pd and Pt-Pd core-shell nanoparticles. Science 322:932–934
54. Arikan T, Kannan AM, Kadirgan F (2013) Binary Pt-Pd and ternary Pt-Pd-Ru nanoelectrocatalysts for direct methanol fuel cells. Int J Hydrogen Energy 38:2900–2907
55. Ghosh S, Sahu RK, Raj CR (2012) Pt-Pd alloy nanoparticle-decorated carbon nanotubes: a durable and methanol tolerant oxygen reduction electrocatalyst. Nanotechnology 23:385602–285610
56. Zhao JA, Manthiram A (2011) Preleached Pd-Pt-Ni and binary Pd-Pt electrocatalysts for oxygen reduction reaction in proton exchange membrane fuel cells. Appl Catal B Environ 101:660–668
57. Long NV, Hien TD, Asaka T, Ohtaki M, Nogami M (2011) Synthesis and characterization of Pt-Pd alloy and core-shell bimetallic nanoparticles for direct methanol fuel cells (DMFCs): enhanced electrocatalytic properties of well-shaped core-shell morphologies and nanostructures. Int J Hydrogen Energy 36:8478–8491

58. Zhou ZM, Shao ZG, Qin XP, Chen XG, Wei ZD, Yi BL (2010) Durability study of Pt-Pd/C as PEMFC cathode catalyst. Int J Hydrogen Energy 35:1719–1726
59. Winjobi O, Zhang ZY, Liang CH, Li WZ (2010) Carbon nanotube supported platinum-palladium nanoparticles for formic acid oxidation. Electrochim Acta 55:4217–4221
60. He W, Liu JY, Qiao YJ, Zou ZQ, Zhang XG, Akins DL, Yang H (2010) Simple preparation of Pd-Pt nanoalloy catalysts for methanol-tolerant oxygen reduction. J Power Sources 195:1046–1050
61. He W, Chen M, Zou ZQ, Li ZL, Zhang XG, Jin SA, You DJ, Pak C, Yang H (2010) Oxygen reduction on Pd_3Pt_1 bimetallic nanoparticles highly loaded on different carbon supports. Appl Catal B Environ 97:347–353
62. Wang WM, Huang QH, Liu JY, Zou ZQ, Zhao MY, Vogel W, Yang H (2009) Surface and structure characteristics of carbon-supported Pd_3Pt_1 bimetallic nanoparticles for methanol-tolerant oxygen reduction reaction. J Catal 266:156–163
63. Kadirgan F, Kannan AM, Atilan T, Beyhan S, Ozenler SS, Suzer S, Yorur A (2009) Carbon supported nano-sized Pt-Pd and Pt-Co electrocatalysts for proton exchange membrane fuel cells. Int J Hydrogen Energy 34:9450–9460
64. Kadirgan F, Beyhan S, Atilan T (2009) Preparation and characterization of nano-sized Pt-Pd/C catalysts and comparison of their electro-activity toward methanol and ethanol oxidation. Int J Hydrogen Energy 34:4312–4320
65. Ficicilar B, Bayrakceken A, Eroglu I (2009) Effect of Pd loading in Pd-Pt bimetallic catalysts doped into hollow core mesoporous shell carbon on performance of proton exchange membrane fuel cells. J Power Sources 193:17–23
66. Li HQ, Sun GQ, Li N, Sun SG, Su DS, Xin Q (2007) Design and preparation of highly active Pt-Pd/C catalyst for the oxygen reduction reaction. J Phys Chem C 111:5605–5617
67. Blair S, Lycke D, Iordache CA (2006) Palladium-platinum alloy anode catalysts for direct formic acid fuel cells. ECS Trans 3:1325–1332
68. Zhou WJ, Zhou ZH, Song SQ, Li WZ, Sun GQ, Tsiakaras P, Xin Q (2003) Pt based anode catalysts for direct ethanol fuel cells. Appl Catal B Environ 46:273–285
69. Li X, Hsing I (2006) Electrooxidation of formic acid on carbon supported Pt_xPd_{1-x} (x = 0-1) nanocatalysts. Electrochim Acta 51:3477–3483
70. Lee YW, Ko AR, Kim DY, Han SB, Park KW (2012) Octahedral Pt-Pd alloy catalysts with enhanced oxygen reduction activity and stability in proton exchange membrane fuel cells. RSC Adv 2:1119–1125
71. Selvaraj V, Grace AN, Alagar M (2009) Electrocatalytic oxidation of formic acid and formaldehyde on nanoparticle decorated single walled carbon nanotubes. J Colloid Interface Sci 333:254–262
72. Lee YW, Ko AR, Han SB, Kim HS, Park KW (2011) Synthesis of octahedral Pt-Pd alloy nanoparticles for improved catalytic activity and stability in methanol electrooxidation. Phys Chem Chem Phys 13:5569–5572
73. Nishanth KG, Sridhar P, Pitchumani S, Shukla AK (2011) A DMFC with methanol-tolerant-carbon-supported-Pt-Pd-alloy cathode. J Electrochem Soc 158:B871–B876
74. Antolini E, Zignani SC, Santos SF, Gonzalez ER (2011) Palladium-based electrodes: a way to reduce platinum content in polymer electrolyte membrane fuel cells. Electrochim Acta 56:2299–2305
75. Lopes T, Antolini E, Gonzalez ER (2008) Carbon supported Pt-Pd alloy as an ethanol tolerant oxygen reduction electrocatalyst for direct ethanol fuel cells. Int J Hydrogen Energy 33:5563–5570
76. Guo SJ, Dong SJ, Wang EK (2009) Polyaniline/Pt hybrid nanofibers: high-efficiency nanoelectrocatalysts for electrochemical devices. Small 5:1869–1876
77. Chen HS, Liang YT, Chen TY, Tseng YC, Liu CW, Chung SR, Hsieh CT, Lee CE, Wang KW (2014) Graphene-supported Pt and PtPd nanorods with enhanced electrocatalytic performance for the oxygen reduction reaction. Chem Commun 50:11165–11168

78. Solla-Gullon J, Rodes A, Montiel V, Aldaz A, Clavilier J (2003) Electrochemical characterisation of platinum-palladium nanoparticles prepared in a water-in-oil microemulsion. J Electroanal Chem 554:273–284
79. Chen CH, Hwang BJ, Wang GR, Sarma LS, Tang MT, Liu DG, Lee JF (2005) Nucleation and growth mechanism of Pd/Pt bimetallic clusters in sodium bis(2-ethylhexyl)sulfosuceinate (AOT) reverse micelles as studied by in situ X-ray absorption spectroscopy. J Phys Chem B 109:21566–21575
80. Escudero MJ, Hontanon E, Schwartz S, Boutonnet M, Daza L (2002) Development and performance characterisation of new electrocatalysts for PEMFC. J Power Sources 106:206–214
81. Zhang H, Xu XQ, Gu P, Li CY, Wu P, Cai CX (2011) Microwave-assisted synthesis of graphene-supported Pd_1Pt_3 nanostructures and their electrocatalytic activity for methanol oxidation. Electrochim Acta 56:7064–7070
82. Zhang H, Yin YJ, Hu YJ, Li CY, Wu P, Wei SH, Cai CX (2010) Pd@Pt core-shell nanostructures with controllable composition synthesized by a microwave method and their enhanced electrocatalytic activity toward oxygen reduction and methanol oxidation. J Phys Chem C 114:11861–11867
83. Xia H, Wang D (2008) Fabrication of macroscopic freestanding films of metallic nanoparticle monolayers by interfacial self-assembly. Adv Mater 20:4253–4256
84. Liang HW, Cao XA, Zhou F, Cui CH, Zhang WJ, Yu SH (2011) A free-standing Pt-nanowire membrane as a highly stable electrocatalyst for the oxygen reduction reaction. Adv Mater 23:1467–1471
85. Jin YD, Dong SJ (2002) Diffusion-limited, aggregation-based, mesoscopic assembly of roughened core shell bimetallic nanoparticles into fractal networks at the air-water interface. Angew Chem Int Ed 41:1040–1044
86. Shi HY, Hu B, Yu XC, Zhao RL, Ren XF, Liu SL, Liu JW, Feng M, Xu AW, Yu SH (2010) Ordering of disordered nanowires: spontaneous formation of highly aligned, ultralong Ag nanowire films at oil-water-air interface. Adv Funct Mater 20:958–964
87. Kang YJ, Ye XC, Chen J, Cai Y, Diaz RE, Adzic RR, Stach EA, Murray CB (2013) Design of Pt-Pd binary superlattices exploiting shape effects and synergistic effects for oxygen reduction reactions. J Am Chem Soc 135:42–45
88. Wu HX, Li HJ, Zhai YJ, Xu XL, Jin YD (2012) Facile synthesis of free-standing Pd-based nanomembranes with enhanced catalytic performance for methanol/ethanol oxidation. Adv Mater 24:1594–1597
89. Liu Y, Chi MF, Mazumder V, More KL, Soled S, Henao JD, Sun SH (2011) Composition-controlled synthesis of bimetallic PdPt nanoparticles and their electro-oxidation of methanol. Chem Mater 23:4199–4203
90. Lim B, Wang JG, Camargo PHC, Cobley CM, Kim MJ, Xia YN (2009) Twin-induced growth of palladium-platinum alloy nanocrystals. Angew Chem Int Ed 48:6304–6308
91. Papageorgopoulos DC, Keijzer M, Veldhuis JBJ, de Bruijn FA (2002) CO tolerance of Pd-rich platinum palladium carbon-supported electrocatalysts-Proton exchange membrane fuel cell applications. J Electrochem Soc 149:A1400–A1404
92. Yi QF, Huang W, Liu XP, Xu GR, Zhou ZH, Chen AC (2008) Electroactivity of titanium-supported nanoporous Pd-Pt catalysts towards formic acid oxidation. J Electroanal Chem 619:197–205
93. Huang D, Yuan Q, Wang HH, Zhou ZY (2014) Facile synthesis of PdPt nanoalloys with sub-2.0 nm islands as robust electrocatalysts for methanol oxidation. Chem Commun 50:13551–13554
94. Yin AX, Min XQ, Zhang YW, Yan CH (2011) Shape-selective synthesis and facet-dependent enhanced electrocatalytic activity and durability of monodisperse sub-10 nm Pt-Pd tetrahedrons and cubes. J Am Chem Soc 133:3816–3819

95. Lu YZ, Jiang YY, Wu HB, Chen W (2013) Nano-PtPd cubes on graphene exhibit enhanced activity and durability in methanol electrooxidation after CO stripping-cleaning. J Phys Chem C 117:2926–2938
96. Lu YZ, Jiang YY, Chen W (2014) Graphene nanosheet-tailored PtPd concave nanocubes with enhanced electrocatalytic activity and durability for methanol oxidation. Nanoscale 6:3309–3315
97. Guo SJ, Dong SJ, Wang EK (2008) A general method for the rapid synthesis of hollow metallic or bimetallic nanoelectrocatalysts with urchinlike morphology. Chem Eur J 14:4689–4695
98. Yang JH, Lee JY, Zhang QB, Zhou WJ, Liu ZL (2008) Carbon-supported pseudo-core-shell Pd-Pt nanoparticles for ORR with and without methanol. J Electrochem Soc 155:B776–B781
99. Liu B, Li HY, Die L, Zhang XH, Fan Z, Chen JH (2009) Carbon nanotubes supported PtPd hollow nanospheres for formic acid electrooxidation. J Power Sources 186:62–66
100. Zhou XM, Fan LZ (2010) Pt/Pd alloy nanoparticles composed of bimetallic nanobowls Synthesis, characterization and electrocatalytic activities. Electrochim Acta 55:8111–8115
101. Chen ZW, Waje M, Li WZ, Yan YS (2007) Supportless Pt and PtPd nanotubes as electrocatalysts for oxygen-reduction reactions. Angew Chem Int Ed 46:4060–4063
102. Zhang H, Jin MS, Wang JG, Li WY, Camargo PHC, Kim MJ, Yang DR, Xie ZX, Xia YA (2011) Synthesis of Pd-Pt bimetallic nanocrystals with a concave structure through a bromide-induced galvanic replacement reaction. J Am Chem Soc 133:6078–6089
103. Zhang H, Jin MS, Liu HY, Wang JG, Kim MJ, Yang DR, Xie ZX, Liu JY, Xia YN (2011) Facile synthesis of Pd-Pt alloy nanocages and their enhanced performance for preferential oxidation of CO in excess hydrogen. ACS Nano 5:8212–8222
104. Lu YZ, Jiang YY, Chen W (2013) PtPd porous nanorods with enhanced electrocatalytic activity and durability for oxygen reduction reaction. Nano Energy 2:836–844
105. Huang XQ, Zhang HH, Guo CY, Zhou ZY, Zheng NF (2009) Simplifying the creation of hollow metallic nanostructures: One-pot synthesis of hollow palladium/platinum single-crystalline nanocubes. Angew Chem Int Ed 48:4808–4812
106. Bauer E, Vandermerwe JH (1986) Structure and growth of crystalline superlattices-from monolayer to superlattice. Phys Rev B 33:3657–3671
107. Fan FR, Liu DY, Wu YF, Duan S, Xie ZX, Jiang ZY, Tian ZQ (2008) Epitaxial growth of heterogeneous metal nanocrystals: From gold nano-octahedra to palladium and silver nanocubes. J Am Chem Soc 130:6949–6951
108. Beard KD, Van Zee JW, Monnier JR (2009) Preparation of carbon-supported Pt-Pd electrocatalysts with improved physical properties using electroless deposition methods. Appl Catal B Environ 88:185–193
109. Long NV, Asaka T, Matsubara T, Nogami M (2011) Shape-controlled synthesis of Pt-Pd core shell nanoparticles exhibiting polyhedral morphologies by modified polyol method. Acta Mater 59:2901–2907
110. Long NV, Ohtaki M, Hien TD, Randy J, Nogami M (2011) A comparative study of Pt and Pt-Pd core-shell nanocatalysts. Electrochim Acta 56:9133–9143
111. Zhang L, Zhang JW, Jiang ZY, Xie SF, Jin MS, Han XG, Kuang Q, Xie ZX, Zheng LS (2011) Facile syntheses and electrocatalytic properties of porous Pd and its alloy nanospheres. J Mater Chem 21:9620–9625
112. Jung DH, Bae SJ, Kim SJ, Nahm KS, Kim P (2011) Effect of the Pt precursor on the morphology and catalytic performance of Pt-impregnated on Pd/C for the oxygen reduction reaction in polymer electrolyte fuel cells. Int J Hydrogen Energy 36:9115–9122
113. Nguyen VL, Ohtaki M, Matsubara T, Cao MT, Nogami M (2012) New experimental evidences of Pt-Pd bimetallic nanoparticles with core-shell configuration and highly fine-ordered nanostructures by high-resolution electron transmission microscopy. J Phys Chem C 116:12265–12274
114. Liu L, Samjeske G, Nagamatsu S, Sekizawa O, Nagasawa K, Takao S, Imaizumi Y, Yamamoto T, Uruga T, Iwasawa Y (2012) Enhanced oxygen reduction reaction activity

and characterization of Pt-Pd/C bimetallic fuel cell catalysts with Pt-enriched surfaces in acid media. J Phys Chem C 116:23453–23464
115. Li YJ, Wang ZW, Chiu CY, Ruan LY, Yang WB, Yang Y, Palmer RE, Huang Y (2012) Synthesis of bimetallic Pt-Pd core-shell nanocrystals and their high electrocatalytic activity modulated by Pd shell thickness. Nanoscale 4:845–851
116. Habas SE, Lee H, Radmilovic V, Somorjai GA, Yang P (2007) Shaping binary metal nanocrystals through epitaxial seeded growth. Nat Mater 6:692–697
117. Guo SJ, Dong SJ, Wang EK (2010) Pt/Pd bimetallic nanotubes with petal-like surfaces for enhanced catalytic activity and stability towards ethanol electrooxidation. Energy Environ Sci 3:1307–1310
118. Lim BW, Lu XM, Jiang MJ, Camargo PHC, Cho EC, Lee EP, Xia YN (2008) Facile synthesis of highly faceted multioctahedral Pt nanocrystals through controlled overgrowth. Nano Lett 8:4043–4047
119. Jiang MJ, Lim B, Tao J, Camargo PHC, Ma C, Zhu YM, Xia YN (2010) Epitaxial overgrowth of platinum on palladium nanocrystals. Nanoscale 2:2406–2411
120. Bai S, Wang C, Deng M, Gong M, Bai Y, Jiang J, Xiong YJ (2014) Surface polarization matters: enhancing the hydrogen-evolution reaction by shrinking Pt Shells in Pt–Pd–Graphene stack structures. Angew Chem Int Ed 126:12316–12320
121. Zhang H, Jin MS, Wang JG, Kim MJ, Yang DR, Xia YN (2011) Nanocrystals composed of alternating shells of Pd and Pt can be obtained by sequentially adding different precursors. J Am Chem Soc 133:10422–10425
122. Lim B, Jiang MJ, Camargo PHC, Cho EC, Tao J, Lu XM, Zhu YM, Xia YN (2009) Pd-Pt bimetallic nanodendrites with high activity for oxygen reduction. Science 324:1302–1305
123. Lee HJ, Habas SE, Somorjai GA, Yang PD (2008) Localized Pd overgrowth on cubic Pt nanocrystals for enhanced electrocatalytic oxidation of formic acid. J Am Chem Soc 130:5406–5407
124. Lim B, Jiang MJ, Yu T, Camargo PHC, Xia YN (2010) Nucleation and growth mechanisms for Pd-Pt bimetallic nanodendrites and their electrocatalytic properties. Nano Res 3:69–80
125. Guo SJ, Dong SJ, Wang EK (2010) Ultralong Pt-on-Pd bimetallic nanowires with nanoporous surface: nanodendritic structure for enhanced electrocatalytic activity. Chem Commun 46:1869–1871
126. Peng ZM, Yang H (2009) Synthesis and oxygen reduction electrocatalytic property of Pt-on-Pd bimetallic heteronanostructures. J Am Chem Soc 131:7542–7543
127. Guo SJ, Dong SJ, Wang EK (2010) Three-dimensional Pt-on-Pd bimetallic nanodendrites supported on graphene nanosheet: facile synthesis and used as an advanced nanoelectrocatalyst for methanol oxidation. ACS Nano 4:547–555
128. Wang L, Nemoto Y, Yamauchi Y (2011) Direct synthesis of spatially-controlled Pt-on-Pd bimetallic nanodendrites with superior electrocatalytic activity. J Am Chem Soc 133:9674–9677
129. Serpell CJ, Cookson J, Ozkaya D, Beer PD (2011) Core@shell bimetallic nanoparticle synthesis via anion coordination. Nat Chem 3:478–483
130. Lee H, Habas SE, Kweskin S, Butcher D, Somorjai GA, Yang PD (2006) Morphological control of catalytically active platinum nanocrystals. Angew Chem Int Ed 45:7824–7828
131. Climent V, Markovic NM, Ross PN (2000) Kinetics of oxygen reduction on an epitaxial film of palladium on Pt(111). J Phys Chem B 104:3116–3120
132. Arenz M, Schmidt TJ, Wandelt K, Ross PN, Markovic NM (2003) The oxygen reduction reaction on thin palladium films supported on a Pt(111) electrode. J Phys Chem B 107:9813–9819
133. Babu PK, Kim HS, Chung JH, Oldfield E, Wieckowski A (2004) Bonding and motional aspects of CO adsorbed on the surface of Pt nanoparticles decorated with Pd. J Phys Chem B 108:20228–20232

134. Zhao MC, Rice C, Masel RI, Waszczuk P, Wieckowski A (2004) Kinetic study of electro-oxidation of formic acid on spontaneously-deposited Pt/Pd nanoparticles-CO tolerant fuel cell chemistry. J Electrochem Soc 151:A131–A136
135. Jayashree RS, Spendelow JS, Yeom J, Rastogi C, Shannon MA, Kenis PJA (2005) Characterization and application of electrodeposited Pt, Pt/Pd, and Pd catalyst structures for direct formic acid micro fuel cells. Electrochim Acta 50:4674–4682
136. Grace AN, Pandian K (2006) Pt, Pt-Pd and Pt-Pd/Ru nanoparticles entrapped polyaniline electrodes—a potent electrocatalyst towards the oxidation of glycerol. Electrochem Commun 8:1340–1348
137. Selvaraj V, Alagar M, Hamerton I (2006) Electrocatalytic properties of monometallic and bimetallic nanoparticles-incorporated polypyrrole films for electro-oxidation of methanol. J Power Sources 160:940–948
138. Selvaraj V, Alagar M, Hamerton I (2007) Nanocatalysts impregnated polythiophene electrodes for the electrooxidation of formic acid. Appl Catal B Environ 73:172–179
139. Xu Y, Lin X (2007) Facile fabrication and electrocatalytic activity of $Pt_{0.9}$ $Pd_{0.1}$alloy film catalysts. J Power Sources 170:13–19
140. Galal A, Atta NF, Darwish SA, Ali SM (2008) Electrodeposited metals at conducting polymer electrodes. II: Study of the oxidation of methanol at poly(3-methylthiophene) modified with Pt-PdCo-catalyst. Top Catal 47:73–83
141. Zhou ZL, Kang TF, Zhang Y, Cheng SY (2009) Electrochemical sensor for formaldehyde based on Pt-Pd nanoparticles and a Nafion-modified glassy carbon electrode. Microchim Acta 164:133–138
142. Mahapatra SS, Dutta A, Datta J (2010) Temperature effect on the electrode kinetics of ethanol oxidation on Pd modified Pt electrodes and the estimation of intermediates formed in alkali medium. Electrochim Acta 55:9097–9104
143. Mahapatra SS, Dutta A, Datta J (2011) Temperature dependence on methanol oxidation and product formation on Pt and Pd modified Pt electrodes in alkaline medium. Int J Hydrogen Energy 36:14873–14883
144. Yang X, Yang QD, Xu J, Lee CS (2012) Bimetallic PtPd nanoparticles on Nafion-graphene film as catalyst for ethanol electro-oxidation. J Mater Chem 22:8057–8062
145. Vidal-Iglesias FJ, Solla-Gullon J, Herrero E, Aldaz A, Feliu JM (2010) Pd adatom decorated (100) preferentially oriented Pt nanoparticles for formic acid electrooxidation. Angew Chem Int Ed 49:6998–7001
146. Zhang JL, Vukmirovic MB, Xu Y, Mavrikakis M, Adzic RR (2005) Controlling the catalytic activity of platinum-monolayer electrocatalysts for oxygen reduction with different substrates. Angew Chem Int Ed 44:2132–2135
147. Zhang J, Mo Y, Vukmirovic M, Klie R, Sasaki K, Adzic R (2004) Platinum monolayer electrocatalysts for O_2 reduction: Pt monolayer on Pd (111) and on carbon-supported Pd nanoparticles. J Phys Chem B 108:10955–10964
148. Adzic RR, Zhang J, Shao M, Sasaki K, Vukmirovic M, Uribe FA (2006) Platinum and mixed platinum-metal monolayer fuel cell electrocatalysts: design, activity and long-term performance stability. ECS Trans 3:31–36
149. Vukmirovic MB, Zhang J, Sasaki K, Nilekar AU, Uribe F, Mavrikakis M, Adzic RR (2007) Platinum monolayer electrocatalysts for oxygen reduction. Electrochim Acta 52:2257–2263
150. Bliznakov ST, Vukmirovic MB, Yang L, Sutter EA, Adzic RR (2012) Pt Monolayer on electrodeposited Pd nanostructures: advanced cathode catalysts for PEM fuel cells. J Electrochem Soc 159:F501–F506
151. Sasaki K, Naohara H, Cai Y, Choi YM, Liu P, Vukmirovic MB, Wang JX, Adzic RR (2010) Core-protected platinum monolayer shell high-stability electrocatalysts for fuel-cell cathodes. Angew Chem Int Ed 49:8602–8607
152. Koenigsmann C, Santulli AC, Gong KP, Vukmirovic MB, Zhou WP, Sutter E, Wong SS, Adzic RR (2011) Enhanced electrocatalytic performance of processed, ultrathin, supported

Pd-Pt core-shell nanowire catalysts for the oxygen reduction reaction. J Am Chem Soc 133:9783–9795
153. Wang JX, Inada H, Wu LJ, Zhu YM, Choi YM, Liu P, Zhou WP, Adzic RR (2009) Oxygen reduction on well-defined core-shell nanocatalysts: particle size, facet, and Pt shell thickness effects. J Am Chem Soc 131:17298–17302
154. Shao MH, He GN, Peles A, Odell JH, Zeng J, Su D, Tao J, Yu T, Zhu YM, Xia YN (2013) Manipulating the oxygen reduction activity of platinum shells with shape-controlled palladium nanocrystal cores. Chem Commun 49:9030–9032
155. Seweryn J, Lewera A (2012) Electrooxidation of ethanol on carbon-supported Pt-Pd nanoparticles. J Power Sources 205:264–271
156. Ignaszak A, Song C, Zhu W, Wang YJ, Zhang J, Bauer A, Baker R, Neburchilov V, Ye S, Campbell S (2012) Carbon–$Nb_{0.07}Ti_{0.93}O_2$ composite supported Pt–Pd electrocatalysts for PEM fuel cell oxygen reduction reaction. Electrochim Acta 75:220–228
157. Lopes PP, Ticianelli EA, Varela H (2011) Potential oscillations in a proton exchange membrane fuel cell with a Pd-Pt/C anode. J Power Sources 196:84–89
158. Kim KH, Yu JK, Lee HS, Choi JH, Noh SY, Yoon SK, Lee CS, Hwang TS, Rhee YW (2007) Preparation of Pt-Pd catalysts for direct formic acid fuel cell and their characteristics. Korean J Chem Eng 24:518–521
159. Parinyaswan A, Pongstabodee S, Luengnaruemitchai A (2006) Catalytic performances of Pt-Pd/CeO_2 catalysts for selective CO oxidation. Int J Hydrogen Energy 31:1942–1949
160. Koutsopoulos S, Johannessen T, Eriksen KM, Fehrmann R (2006) Titania-supported Pt and Pt-Pd nanoparticle catalysts for the oxidation of sulfur dioxide. J Catal 238:206–213
161. Mougenot M, Caillard A, Brault P, Baranton S, Coutanceau C (2011) High performance plasma sputtered PdPt fuel cell electrodes with ultra low loading. Int J Hydrogen Energy 36:8429–8434
162. Schmidt TJ, Markovic NM, Stamenkovic V, Ross PN, Attard GA, Watson DJ (2002) Surface characterization and electrochemical behavior of well-defined Pt-Pd{111} single-crystal surfaces: a comparative study using Pt{111} and palladium-modified Pt{111} electrodes. Langmuir 18:6969–6975
163. Ohashi M, Beard KD, Ma SG, Blom DA, St-Pierre J, Van Zee JW, Monnier JR (2010) Electrochemical and structural characterization of carbon-supported Pt-Pd bimetallic electrocatalysts prepared by electroless deposition. Electrochim Acta 55:7376–7384
164. Wang C, Peng B, Xie HN, Zhang HX, Shi FF, Cai WB (2009) Facile fabrication of Pt, Pd and Pt-Pd alloy films on Si with tunable infrared internal reflection absorption and synergetic electrocatalysis. J Phys Chem C 113:13841–13846
165. Cangul B, Zhang LC, Aindow M, Erkey C (2009) Preparation of carbon black supported Pd, Pt and Pd-Pt nanoparticles using supercritical CO_2 deposition. J Supercrit Fluids 50:82–90
166. Yen CH, Shimizu K, Lin YY, Bailey F, Cheng IF, Wai CM (2007) Chemical fluid deposition of Pt-based bimetallic nanoparticles on multiwalled carbon nanotubes for direct methanol fuel cell application. Energy Fuel 21:2268–2271
167. Arico AS, Srinivasan S, Antonucci V (2001) DMFCs: from fundamental aspects to technology development. Fuel Cells 1:133–161
168. Choi WC, Jeon MK, Kim YJ, Woo SI, Hong WH (2004) Development of enhanced materials for direct-methanol fuel cell by combinatorial method and nanoscience. Catal Today 93–95:517–522
169. Koenigsmann C, Wong SS (2011) One-dimensional noble metal electrocatalysts: a promising structural paradigm for direct methanol fuel cells. Energy Environ Sci 4:1161–1176
170. Shukla AK, Ravikumar MK, Gandhi KS (1998) Direct methanol fuel cells for vehicular applications. J Solid State Electrochem 2:117–122
171. Leger JM (2001) Mechanistic aspects of methanol oxidation on platinum-based electrocatalysts. J Appl Electrochem 31:767–771
172. Zhang XY, Lu W, Da JY, Wang HT, Zhao DY, Webley PA (2009) Porous platinum nanowire arrays for direct ethanol fuel cell applications. Chem Commun 2:195–197

173. Arenz M, Stamenkovic V, Ross PN, Markovic NM (2004) Surface (electro-)chemistry on Pt (111) modified by a pseudomorphic Pd monolayer. Surf Sci 573:57–66
174. Qian W, Hao R, Zhou J, Eastman M, Manhat BA, Sun Q, Goforth AM, Jiao J (2013) Exfoliated graphene-supported Pt and Pt-based alloys as electrocatalysts for direct methanol fuel cells. Carbon 52:595–604
175. Feng JX, Zhang QL, Wang AJ, Wei J, Chen JR, Feng JJ (2014) Caffeine-assisted facile synthesis of platinum@palladium core-shell nanoparticles supported on reduced graphene oxide with enhanced electrocatalytic activity for methanol oxidation. Electrochim Acta 142:343–350
176. Bianchini C, Shen PK (2009) Palladium-based electrocatalysts for alcohol oxidation in half cells and in direct alcohol fuel cells. Chem Rev 109:4183–4206
177. Lamy C, Rousseau S, Belgsir EM, Coutanceau C, Leger JM (2004) Recent progress in the direct ethanol fuel cell: development of new platinum-tin electrocatalysts. Electrochim Acta 49:3901–3908
178. Simoes FC, dos Anjos DM, Vigier F, Leger JM, Hahn F, Coutanceau C, Gonzalez ER, Tremiliosi G, de Andrade AR, Olivi P, Kokoh KB (2007) Electroactivity of tin modified platinum electrodes for ethanol electrooxidation. J Power Sources 167:1–10
179. Yu XW, Pickup PG (2008) Recent advances in direct formic acid fuel cells (DFAFC). J Power Sources 182:124–132
180. Rees NV, Compton RG (2011) Sustainable energy: a review of formic acid electrochemical fuel cells. J Solid State Electrochem 15:2095–2100
181. Rees NV, Compton RG (2012) Sustainable energy: a review of formic acid electrochemical fuel cells. J Solid State Electrochem 16:419–419
182. Grigoriev SA, Lyutikova EK, Martemianov S, Fateev VN (2007) On the possibility of replacement of Pt by Pd in a hydrogen electrode of PEM fuel cells. Int J Hydrogen Energy 32:4438–4442
183. Baranova EA, Miles N, Mercier PH, Le Page Y, Patarachao B (2010) Formic acid electro-oxidation on carbon supported $Pd_xPt_{1-x}(0\geq x\geq 1)$ nanoparticles synthesized via modified polyol method. Electrochim Acta 55:8182–8188
184. Guo SJ, Zhang S, Sun SH (2013) Tuning nanoparticle catalysis for the oxygen reduction reaction. Angew Chem Int Ed 52:8526–8544
185. Jiang YY, Lu YZ, Lv XY, Han DX, Zhang QX, Niu L, Chen W (2013) Enhanced catalytic performance of Pt-free iron phthalocyanine by graphene support for efficient oxygen reduction reaction. ACS Catal 3:1263–1271
186. Bliznakov ST, Vukmirovic MB, Yang L, Sutter EA, Adzic RR (2011) Pt monolayer on electrodeposited Pd nanostructures-advanced cathode catalysts for PEM fuel cells. ECS Trans 41:1055–1066
187. Sasaki K, Wang JX, Naohara H, Marinkovic N, More K, Inada H, Adzic RR (2010) Recent advances in platinum monolayer electrocatalysts for oxygen reduction reaction: Scale-up synthesis, structure and activity of Pt shells on Pd cores. Electrochim Acta 55:2645–2652